

Report No. KFY-FR

May 1990

**CARBON DEPOSITION MODEL FOR
OXYGEN/HYDROCARBON COMBUSTION
(NAS 8-34715)**

**TASK VI: DATA ANALYSIS AND FORMULATION
OF AN EMPIRICAL MODEL**

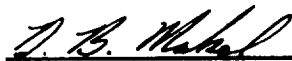
Task VI Final Report

Prepared for

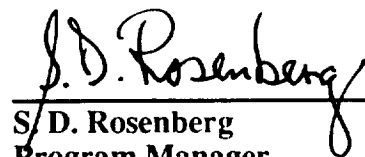
**NATIONAL AERONAUTICS AND SPACE ADMINISTRATION
GEORGE C. MARSHALL SPACE FLIGHT CENTER
HUNTSVILLE, ALABAMA 35812**

Prepared By:

Approved By:



**D. B. Makel
Project Engineer**



**S/ D. Rosenberg
Program Manager**

**Aerojet TechSystems
P.O. Box 13222
Sacramento, California 95813**

FOREWORD

The Carbon Deposition Model for Oxygen-Hydrocarbon Combustion Program (Contract NAS 8-34715) was conducted by Aerojet TechSystems (AT) for the NASA-Marshall Space Flight Center. The Task VI activities described in this final report were conducted from April 1989 to May 1990. Fred Braam was the NASA-Marshall Program Manager. At AT, the program manager for Task VI was Dr. Sanders D. Rosenberg. The project engineer on Task VI was Darby B. Makel. Major contributions to the model developed on the program were made by Dr. Ian M. Kennedy of the University of California, Davis (UCD). In addition, injector mixing tests were performed at Dr. Kennedy's research laboratory at UCD. Significant contributions were made to the program by the following AT personnel:

Wendelin M. Burkhardt

Darlene Hunt

Shirley J. Reed

Jeffrey C. Schneider

PRECEDING PAGE BLANK NOT FILMED

ABSTRACT

The formation and deposition of carbon (soot) has been studied in the Carbon Deposition Model for Oxygen-Hydrocarbon Combustion Program (Contract NAS 8-34715.) An empirical, 1-dimensional model for predicting soot formation and deposition in LO₂/hydrocarbon gas generators/preburners has been derived. The experimental data required to anchor the model have been identified and a test program to obtain the data has been defined. In support of the model development, cold flow mixing experiments using a high injection density injector have been performed. The purpose of this investigation was to advance the state-of-the-art in LO₂/hydrocarbon gas generator design by developing a reliable engineering model of gas generator operation. The model has been formulated to account for the influences of fluid dynamics, chemical kinetics, and gas generator hardware design on soot formation and deposition.

CONTENTS

	<u>Page</u>
1.0 INTRODUCTION	1
1.1 Background	1
1.2 Objectives	5
2.0 SUMMARY	6
3.0 CONCLUSIONS AND RECOMMENDATIONS	8
3.1 Conclusions	8
3.2 Recommendations	9
4.0 TECHNICAL DISCUSSION	10
4.1 Fundamentals of Soot Formation and Deposition	10
4.2 Model Formulation	14
4.2.1 Overall Methodology	18
4.2.2 Identification of Model Parameters	20
4.2.3 Soot Formation Model	20
4.2.4 Soot Deposition Model	30
4.2.5 1-D Flow Model	37
4.2.6 Combustion Kinetics Model	38
4.3 Injector Mixing Experiments	39
4.3.1 Test Apparatus	41
4.3.2 Test Summary	46
4.4 Model Validation Program	50
4.4.1 Validation Program Tasks	50
4.4.2 Diagnostics and Hardware Requirements	58
REFERENCES	73

FIGURES

		Page
1	Gas Generator Operating Limits Defined in First Phase of Program	3
2	Soot Formation Processes	11
3	Soot Deposition Mechanism	13
4	Modeling Approaches for Low Mixture Ratio Combustion and Carbon Deposition Model	15
5	Elements of the Low Mixture Ratio Combustion and Carbon Deposition Model	19
6	Parameters Affecting Soot Formation and Deposition	21
7	High Injector Mixing Rates May Suppress Soot Particle Nucleation	22
8	Prediction of Soot Volume Fraction for Task V LO ₂ /Propane Tests	29
9	Pressure Drop Due to Carbon Deposition Measured During Task V	31
10	Prediction of Carbon Deposition as a Function of Turbine Inlet Nozzle Diameter for Constant Flowrate of 2.0 lbm/sec	35
11	Predicted Effect of Wall Temperature on Carbon Deposition for Gas Temperature of 1520 F in a 20:1 Contraction Ratio Nozzle with LO ₂ /RP-1 at MR=0.4 and 2 lbm/sec	36
12	High Injection Density Injector	40
13	Setup For 2-D Rayleigh Imaging of Injector Mixing	42
14	Experimental Apparatus For 2-D Rayleigh Scatter Imaging of Injector Mixing	43
15	Diagnostic Chamber Assembly	45
16	2-D Images of Injector Mixing at MR=0.3 and MR=0.5	49
17	Model Verification Program	51
18	Data Requirements for Model Validation	52
19	Fundamentals of Laser Diagnostics for Model Validation	54
20	Controlled Low Mixture Ratio Combustion Tests	57

21	Single Element Injector Testing	61
22	Subscale Hardware Configuration for Validation Testing	69
23	Conceptual Design of Diagnostic Flange for Simultaneous Extinction and LDV Measurements	70
24	Diagnostic Flange for Soot Deposition Measurement	71

TABLES

I	Calculation of Soot Volume Fraction for Task V LO ₂ /Propane Tests	28
II	Injector Mixing Test Results	47
III	Review of Diagnostics For Model Validation Testing	59

1.0 INTRODUCTION

This final report describes Aerojet TechSystems' (AT) activities for *Task VI: Data Analysis and Formulation of an Empirical Model* for the Carbon Deposition Model for Oxygen/Hydrocarbon Combustion Program, NAS 8-34715. The objective of Task VI was to develop a framework of an empirical Low Mixture Ratio Combustion and Carbon Deposition Model and establish a plan for validating the model. The model which has been developed is based on phenomenological descriptions of soot formation, growth, transport, and deposition. Data to construct the model has been derived from three sources.

1. Carbon deposition characteristics of LO₂/methane, LO₂/propane, and LO₂/RP-1 determined from the Task V gas generator tests.
2. Open literature; in particular, work conducted during the past eight years.
3. Injector mixing data obtained using nonintrusive laser diagnostics on cold flow tests conducted with test hardware.

1.1 BACKGROUND

Advanced engine studies have indicated that significant mission performance and life cycle cost benefits are associated with LO₂/hydrocarbon propellant engine systems. Potential long range applications include a liquid rocket booster for the space shuttle, a block II propellant system for OMS and RCS engines on the space shuttle orbitor, an advanced single stage-to-orbit shuttle replacement vehicle, and a heavy lift launch vehicle.

Before the start of the current program in 1982, the development of combustion devices for the next generation of booster engines was hampered because of both the lack of critical data and the existence of contradictory data for both main chamber combustion devices and preburner or gas generator devices. Low pressure hydrocarbon engine data showed that carbon deposition on the chamber wall forms an insulating layer which could be beneficial from a cooling standpoint. The extent of carbon deposition on the main chamber walls may determine an engine's operating pressure capability by minimizing the combustion heat flux at the chamber wall.

In preburners/gas generators, carbon buildup on the turbine blades and nozzles increases operation and maintenance costs and may prohibit the use of heavy hydrocarbon fuels for reusable applications. The design of LO₂/hydrocarbon engines requires an understanding of the factors controlling soot formation and deposition. However, an incomplete data base on low

1.1, Background (cont.)

mixture ratio combustion characteristics and soot deposition rates for LO₂/RP-1 and LO₂/methane, and the lack of data for LO₂/propane, have made it difficult to characterize LO₂/HC combustion for the rational selection of the most promising propellant combination and combustor designs for future engine development programs.

In the past, expendable booster engines, operating with LO₂/RP-1 propellants have been designed (through costly iterations) to operate with excessive carbon deposition. Future reusable engines will not be as tolerant to the performance losses, degraded life, and clean up costs associated with soot formation. The first phase of the program, reported in Reference 1, addressed the generation and deposition of carbon using subscale hardware. LO₂/RP-1 was studied at main chamber mixture ratios. LO₂/RP-1, LO₂/methane, and LO₂/propane were studied at low mixture ratio, gas generator/preburner conditions. One universal test set-up using the same fine pattern triplet injector was used throughout the testing. Carbon deposition during the main chamber operation with LO₂/RP-1 was studied for mixture ratios of 2.0 to 4.0 and chamber pressures of 1000 to 1500 psia (6.89 to 10.34 MPa). Thermal data and visual post-test inspection showed no evidence of carbon deposition on the chamber walls. The deposition of carbon on the turbine simulator tubes during the preburner/gas generator testing was evaluated at mixture ratios of 0.20 to 0.60 and at chamber pressures from 720 to 1650 psia (4.96 to 11.38 MPa). The mixture ratios covered the bulk combustion temperature range of interest for state-of-the-art turbopump machinery, 1300 to 1600 F (978 to 1144 K). The results show that the carbon deposition rate is a strong function of the mixture ratio and a weak function of chamber pressure. Gas generator testing with LO₂/propane revealed a threshold mixture ratio for which carbon deposition begins and becomes very heavy. Carbon deposition was not detected for LO₂/methane at any mixture ratio tested. From the carbon deposition analyses, the turbine drive operating limits were defined for each fuel tested. The data indicate that methane is the only hydrocarbon fuel tested that can be run without carbon deposition over the desired gas generator operating temperature range.

The results from the first phase of testing for the carbon deposition and gas temperatures as a function of mixture ratio are summarized in Figure 1. The curves on each plot indicate the measured gas temperature as a function of mixture ratio tested for each fuel. Superimposed on each plot is the desired temperature range for the operation of state-of-the-art turbine drives. The highlighted area indicates the region where operation for each fuel will not incur or at least minimally incur carbon buildup. The intersection of the highlighted area with the area delineating the desired temperature range indicates the region of acceptable performance for a gas generator for each fuel. Figure 1 indicates that LO₂/RP-1 cannot be operated in the desirable temperature

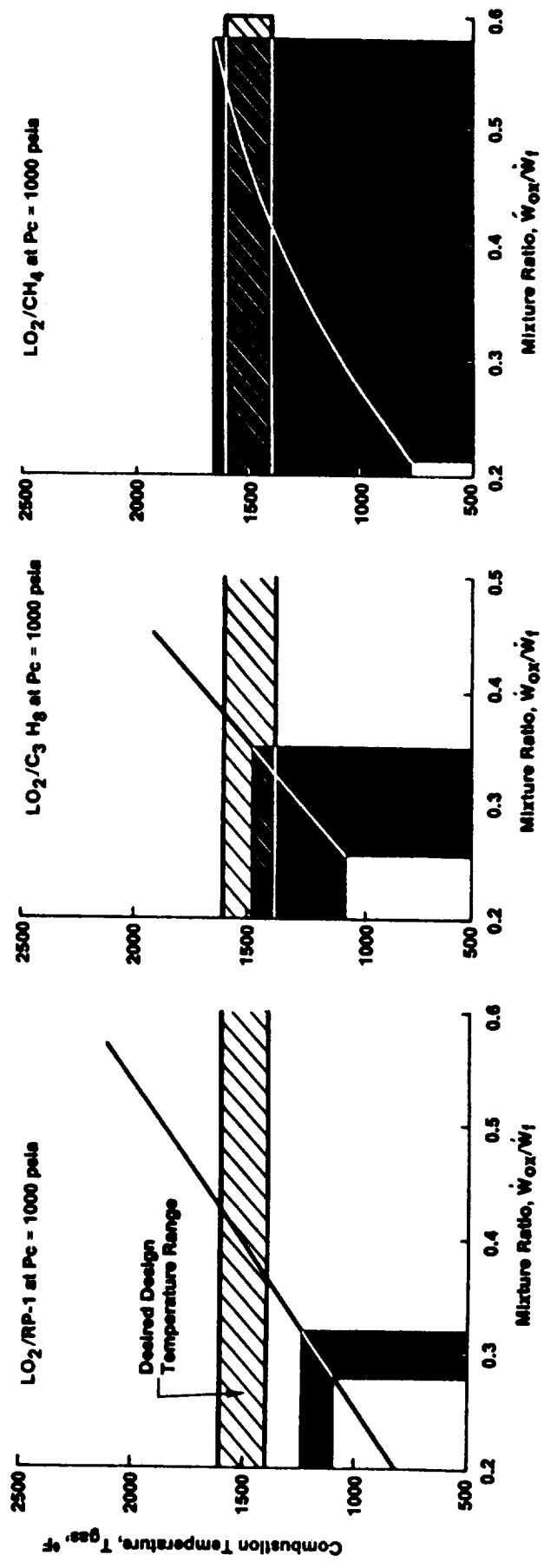


Figure 1. Gas Generator Operating Limits Defined in First Phase of Program

1.1, Background (cont.)

range for gas generators without incurring undesirable carbon buildup. LO₂/propane can be operated in the desired temperature range up to a maximum of 1500 F (1088 K). Operation with LO₂/methane is unrestricted over the desired gas generator operating temperature range.

The second phase of the program, reported in Reference 2, extended the LO₂/methane database by investigating fuel purity and injection density effects on carbon deposition at gas generator conditions. To test the effect of fuel purity, LO₂/liquidified natural gas (LNG) was tested using the same fine pattern injector as the earlier testing. The LO₂/LNG gas generator/preburner testing was performed at mixture ratios between 0.24 and 0.58 and chamber pressures from 840 to 1370 psia (5.8 to 9.4 MPa). A coarse element triplet injector was constructed to permit testing at approximately full scale injection densities (10 times the injection densities used in the earlier testing). The new injector was used for high injection density LO₂/methane testing at mixture ratios from 0.23 to 0.81 and chamber pressures from 925 to 2210 psia (6.4 to 15.2 MPa). No detectable carbon deposition was measured for the LO₂/LNG and the high injection density LO₂/methane tests.

While the results of the earlier phases of the program successfully characterized the carbon deposition differences among the three hydrocarbon fuels tested, sufficient data to develop a model to predict soot formation and deposition were not obtained. It was recommended at the end of the second phase of testing that the effects of hardware geometry, injector design, and combustion kinetics be investigated as potential means of reducing the high soot deposition rates measured for LO₂/RP-1 and LO₂/propane. The objective of the investigation would be to develop an engineering model for gas generator design which can define conditions leading to minimum carbon deposition.

Several advances in the application of laser diagnostic techniques to practical combustion devices have occurred in the past 10 years. Application of these techniques to gas generator combustion should enable the combustion and carbon deposition to be empirically modeled using detailed measurements of local flow and combustion parameters. Prior attempts to model gas generator soot formation and deposition have proven inadequate for design purposes because the soot concentration in the flow, the most important parameter for the model could not be measured. The approach taken in this study has been to formulate a model relating soot formation and deposition to flow and combustion parameters such as propellant type, local wall shear stress, turbulence, velocity gradients at the interface of propellant streams from individual fuel and oxidizer injector

1.1, Background (cont.)

elements, and temperature gradients. This approach should yield a model that predicts soot formation and deposition in terms of parameters which can be controlled through hardware design.

1.2 OBJECTIVES

The first objective of the program was to formulate a Low Mixture Ratio Combustion and Carbon Deposition Model based on available data and realistic models for soot formation, growth, transport, and deposition. The second objective was to define an experimental program, based on the use of nonintrusive laser diagnostics to provide the key information needed for verification of the model. The model is intended to be a tool for the design of gas generator components such as injectors and combustion chambers, based on a minimum soot formation criteria. The model will also predict the total soot yield and local carbon deposition as a function of operating conditions and geometry. The experimental program is based on a progression from laboratory scale experiments to high-pressure, single-element injector experiments, and eventually to subscale experiments using the existing test hardware from NAS 8-34715.

2.0 SUMMARY

An empirical model of carbon formation and deposition applicable to LO₂/hydrocarbon gas generators/preburners has been formulated. A literature review has been conducted to review the state-of-the-art in soot formation and deposition modeling. Previous models and test data were evaluated and have been used to construct the model. The purpose of this modeling effort has been to develop a unified methodology for predicting soot formation and deposition rates when designing LO₂/hydrocarbon gas generators. The equations derived for the model can be programmed into a computer code. The empirical constants in the model have been defined and a test program for quantifying these constants and validating the model has been prepared.

The most important physical mechanisms controlling soot formation and deposition at low mixture ratio gas generator conditions are contained in the model. These mechanisms are: (1) inception of solid soot particles from gaseous combustion products, (2) increase in the size and mass of soot particles due to surface reactions with gas phase hydrocarbons and collision with other soot particles, (3) deposition via thermophoresis (i.e. "mass transfer" down a temperature gradient,) and (4) reentrainment and shearing of previously deposited soot at high flow velocities. The derived equations for the model are based on a one-dimensional representation of the flow in the gas generator and turbine drive assembly. The concentration of soot (expressed as the volume of soot per unit volume of flow) is calculated as a function of time. A chemical kinetics model (yet to be defined) for each propellant combination is used to calculate the axial temperature profile and concentration of unburned C₂ and C₃ hydrocarbons at stations down the length of the chamber. Once the axial profile of soot concentration and temperature are known, the deposition rate of soot on the wall at each station is calculated. The deposition rate is determined using a mass transfer analogy to the local heat transfer. The local wall heat transfer coefficients are calculated using existing correlations and are then transformed into soot mass transfer coefficients, which account for the effects of thermophoresis and reentrainment.

A major unknown issue in the modeling of soot formation at low mixture ratio combustion conditions is the effect of injector mixing. The mixing characteristics of the injector determine whether the combustion is primarily premixed (kinetically limited) or diffusion dominated (mixing limited). Depending on the injection pattern, a gas generator may exhibit varying degrees of each type of combustion. The chemical reactions leading to the formation and growth of soot particles are slow reactions relative to the gas phase combustion reactions. These reactions occur on time scales approximately equal to those of the turbulent mixing, and therefore are profoundly affected by the fluid dynamics in the combustion zone. Cold flow tests to assess the mixing characteristics

2.0, Summary (cont.)

of the high injection density injector (considered a conventional gas generator injector design) have been conducted. The tests used molecular scattering of laser light to visualize 2-D cross sections of the flow near the injector face. The tests reveal large zones of unmixed fuel at more than 20 injection orifice diameters downstream of the injector face. Based on these results a particle nucleation rate term dependent on the mean axial turbulent mixing rate has been included in the model.

3.0 CONCLUSIONS AND RECOMMENDATIONS

3.1 CONCLUSIONS

Currently, there is no reliable methodology for predicting soot formation and deposition in LO₂/hydrocarbon gas generators. The processes governing soot formation and deposition are highly dependent on hardware configuration (injector pattern, chamber contour) and operating conditions (MR and Pc.) Therefore, existing test data cannot be directly extended to new designs. The viability of heavy hydrocarbon fuels (RP-1 and propane) for future missions is limited by the present lack of knowledge as to how to design gas generators which produce minimum soot deposition. The initial step in filling this technology void has been taken on this program with the development of the framework of an engineering model for gas generator design.

The equations for an empirical Low Mixture Ratio Combustion and Carbon Deposition Model have been formulated. The model represents a significant advancement over previous approaches to predicting the soot formation and deposition tendencies of LO₂/hydrocarbon gas generators. The model accounts for the fundamental physical processes controlling soot formation and deposition. The advantage of this type of model is that it is applicable to different hardware designs and should be valid over a wide range of operating conditions. The major tradeoff for this type of model is that it requires data types beyond what has been collected to date in order to quantify parameters and validate the model. Specifically, the soot particle inception rate as a function of injector mixing, the soot surface growth rate for the candidate hydrocarbon fuels at elevated pressures, and the soot layer adhesion strength must be determined. These data can be obtained using proven laser-based combustion diagnostic techniques on subscale tests such as those conducted during Task V.

In addition to the development of the model to predict soot formation and deposition, several hypotheses regarding how to reduce or entirely eliminate soot deposition have been deduced during the program. These hypotheses are: (1) the suppression of soot particle nucleation through the use of very rapid mixing of fuel and oxidizer, (2) the suppression of soot surface growth reactions through the use of fuel additives, (3) the reduction of deposition through tailored design of the wall temperature profile. Exploiting one or a combination of these mechanisms through innovative hardware design may result in a "soot free" gas generator design.

3.0, Conclusions and Recommendations (cont.)

3.2 RECOMMENDATIONS

The program has provided considerable data and the framework of an engineering model for the prediction of soot formation and deposition. A systematic program should be initiated to continue the development of the model and perform the required model validation tests as described in the technical summary (Section 4.0). The empirical inputs required by the model should be determined through a progression of controlled experiments. The major component of the test program should be direct measurements of the soot concentration and deposition using the existing Task V test hardware and nonintrusive laser diagnostics. The modular design and known combustion stability characteristics of the existing program hardware make it ideal for validation testing. Laser diagnostic access for the required measurements can be readily accommodated by means of special "diagnostic flanges" which could easily be incorporated into the hardware test configuration. Following the model validation tests, the model should be used to design a high pressure LO₂/hydrocarbon gas generator. This gas generator would be designed to minimize soot formation and deposition and to serve as a baseline design for a future LO₂/hydrocarbon engine development program.

In parallel with the model validation testing, the existing 1-D model should be extended to 2-D or 3-D as a submodel to be integrated into a computation fluid dynamics (CFD) code. CFD is emerging as a necessary design tool for high pressure, high performance engine design and analysis (e.g. SSME product improvement and ALS.) A CFD-based soot formation and deposition model is potentially the ultimate analysis tool for detailed gas generator design. Such a model should greatly reduce the inherent limitations of an empirically based 1-D model. CFD based models of soot formation and transport in turbulent flames have proven successful and appear readily adaptable to current rocket engine combustion codes. Concurrent development of a CFD based model and the empirical model validation tests would maximize test effectiveness and reduce the overall development time of a useful CFD model.

4.0 TECHNICAL DISCUSSION

4.1 FUNDAMENTALS OF SOOT FORMATION AND DEPOSITION

Solid carbon (soot) deposits found in gas generators can be formed by two mechanisms. The first mechanism is pyrolysis of liquid fuel due to droplet heating during combustion. This process, known as coking, results in solid particulates ranging in diameter from 50 to 200 microns. This is the same phenomena which causes carbon deposits when hydrocarbon fuels are used to regeneratively cooled or film cooled thrust chambers. Direct coking of the liquid fuel provides a small contribution to the total solid carbon formation under gas generator combustion conditions. The second, and most important mechanism, is soot formation through gas phase reactions. During this process, nucleation of small soot particles occurs in the fuel rich side of the combustion zones. These particles are very small in diameter, typically 1 to 10 nm, but rapidly grow in size to about 200 nm as they react with excess hydrocarbon molecules. The surface growth reactions typically account for 90 percent of the solid carbon mass deposited in combustors [3].

The soot formation process in a gas generator is illustrated in Figure 2. Discrete injection locations for fuel and oxidizer create hot, fuel rich zones comprised of gaseous fuel and partial vaporized droplets near the local flame fronts where the mixture ratio is stoichiometric. At low mixture ratio conditions, the fuel rich zones must exist. An injector with high mixing rates will be characterized by flame fronts with high surface area and the fuel rich volume of the flow distributed into many small zones. An injector with low mixing is characterized by a flame front with relatively low surface area and large zones of unburned fuel. The unburned, vaporized fuel molecules undergo thermal decomposition resulting in the formation of polycyclic aromatic hydrocarbons (PAHs.) The PAHs are known to be precursors to soot formation although the detailed kinetics of the formation process are unclear [3]. Soot particles are nucleated within the hottest portions of the fuel rich zones. The residence time of a particle in a hot zone is significantly less when the mixing is very rapid. The particle will continue to grow while it is in a region of the flow where the local temperature exceeds 2500 F (1558 K.) Once the soot particle is beyond the flame zone and its temperature is reduced to the typical gas generator bulk exit temperature of 1300 to 1600 F (926 to 1084 K), the particle stops growing. This effect is explained by the fact that the surface growth reactions between the gas phase hydrocarbons and the soot particles, which result in the addition of solid carbon to the particle, are highly temperature dependent. The temperature dependence of the reactions explains why at extremely low mixtures (less than 0.25) little soot is formed. At these

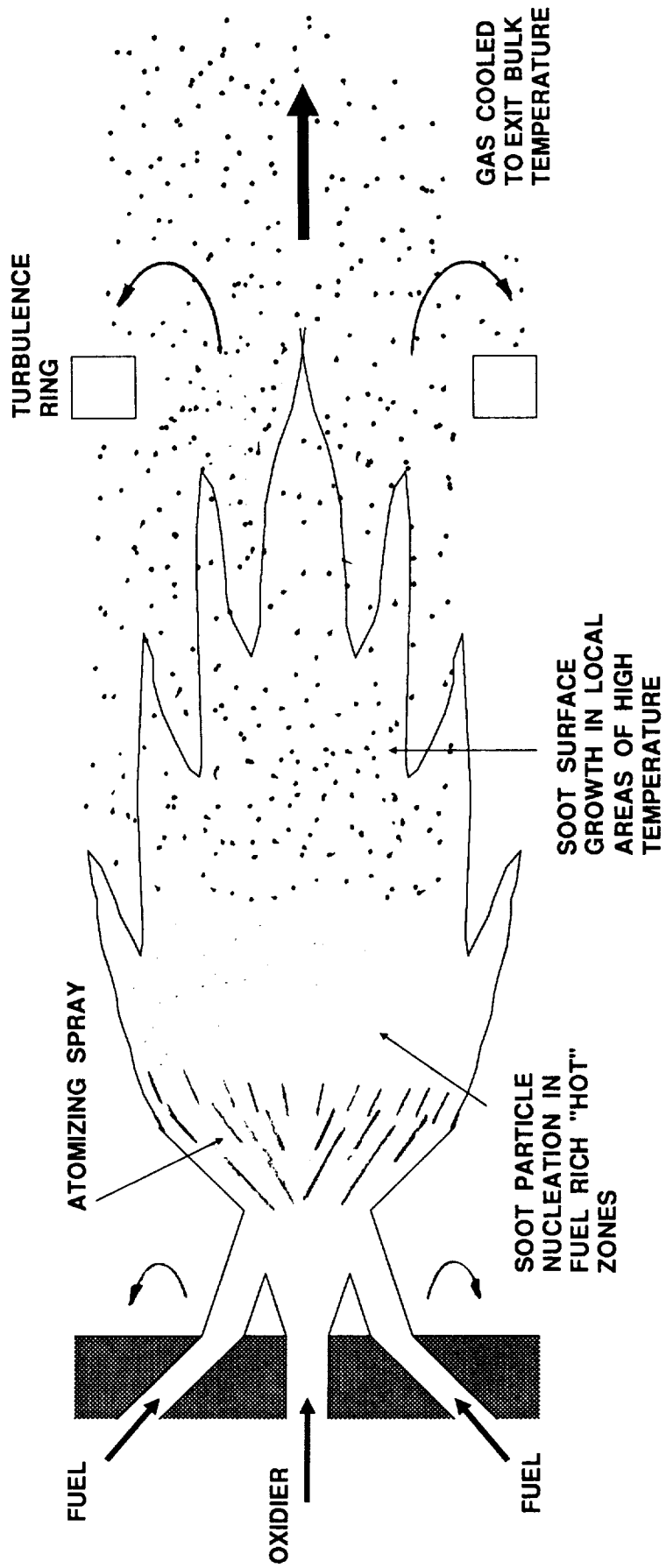


Figure 2. Soot Formation Processes

4.1, Fundamentals of Soot Formation and Deposition (cont.)

conditions, the combustion is so oxidizer deficient that the flame regions are necessarily very small and the heat release is too low to accommodate soot particle nucleation or growth.

The soot deposition processes within gas generators and turbomachinery components are illustrated in Figure 3. Once the combustion gases are thoroughly mixed (usually by a turbulence ring) the flow can be characterized as a hot, nonreacting, particle laden flow. The soot particles in the flow are approximately 200 nm in diameter [3]. Particles of this size are too large to be significantly influenced by diffusion (concentration gradients) and are too small to have sufficient inertia to deviate from the fluid streamlines. The process primarily responsible for soot deposition has been shown to be thermophoresis ("mass transfer down a temperature gradient") [4]. Thermophoresis arises from the fact that a particle in a flow with a temperature gradient is struck with high energy (i.e. high velocity gas molecules) on the hotter side of the particle than on the colder side. The net effect of the imbalance of forces on the particle is a net force propelling the particle across streamlines from a hot gas toward a colder surface [5]. Even when the combustion gases and wall temperatures vary by as little as 5%, thermophoretic deposition is the dominate deposition mechanism, over a factor of 10 greater than diffusional deposition.

As illustrated in Figure 3, the soot deposition patterns in a gas generator show the heaviest deposition in areas of high heat transfer such as stagnation surfaces and nozzles (high velocity regions). At sufficiently high velocities, however, such as in turbine nozzles, the fluid wall shear stress can exceed the adhesion strength of the soot particle to the wall. When the soot adhesion strength is exceeded, reentrainment of soot particles will occur and the net deposition will be reduced in the region. Cyclic differential pressure fluctuations, such as those measured during testing of the Titan I gas generator [1], were probably due to an increasing wall shear stress as the deposition layer built up and the local flow velocity increased, due to a reduction in the flow area. The soot layer would then build up again once some of the layer was sheared away and the local velocity was reduced so that the wall shear stress was less than the average soot layer adhesion strength. The important consequence of the dependence of deposition on wall shear stress is that different gas generator flow geometries will experience different "net deposition," even when the amount of soot formed is the same.

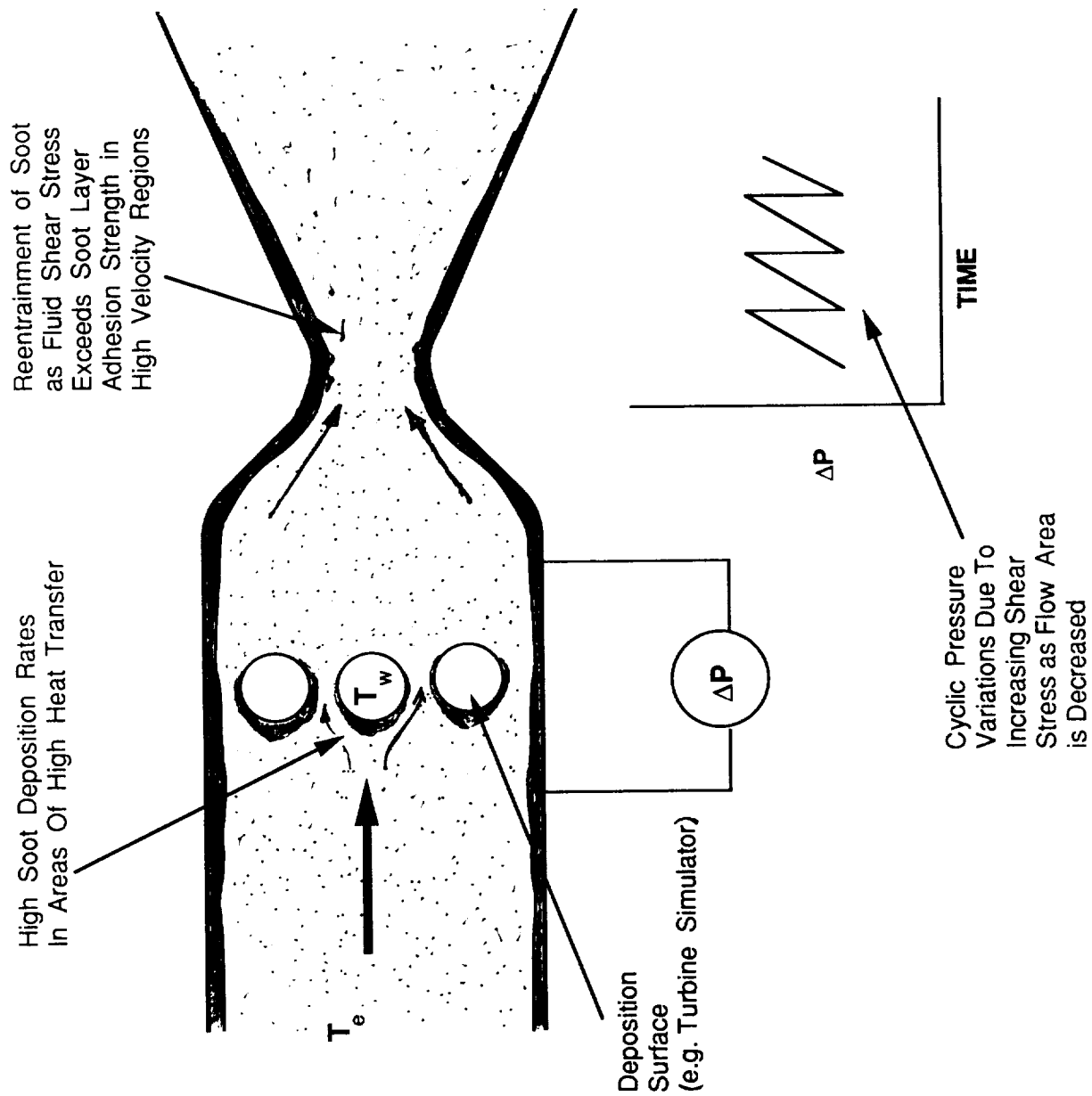


Figure 3. Soot Deposition Mechanism

4.2 MODEL FORMULATION

Approaches for modeling soot formation and deposition are separated into three categories representing different levels of sophistication and applicability. The first level (Level I) consists of single parameter correlations of experimental data. The second level (Level II) consists of one dimensional, lumped-parameter methods in which the flow equations, combustion kinetics, soot formation and deposition are determined at discrete locations along the length of the gas generator and turbine inlet. The most sophisticated modeling (Level III) involves solution of 2-D or 3-D conservation equations for momentum, energy, and soot volume fraction (i.e. volume occupied by soot particle per unit volume of space in the flow field.)

The Level I type models represent existing design tools and describe the complicated physics occurring within a gas generator inadequately [1]. The Level II type models are empirically based analytical models which are useful for design provided sufficient data is obtained to properly adjust the empirical constants. The Level III type models represent the ultimate design and analysis tool, however such modeling at present is limited by the uncertainty of CFD solutions of the two-phase turbulent combustion typical of gas generators. The Level III type models should be useful in modeling controlled tests which may be required to completely develop a Level II type model. A summary of the various models and their relative advantages and disadvantages are summarized in Figure 4 and discussed below.

Level I - Level I type models were extensively summarized in the first Interim Summary Report [1]. These models include the Seader and Wagner carbon deposit correlation and the Rocketdyne correlation of carbon deposit thermal resistance. These types of correlations are based on single parameters (such as mixture ratio and mass flux of combustion gases) and have been developed based on limited data sets. These models are useful from the standpoint of indicating trends in soot formation (e.g. gross MR dependence), but provide no reliable data for developing new gas generator designs. Level I type models offer little potential for advancing the state-of-the-art in gas generator design.

Level II - Level II type models appear to have the greatest potential as a near-term engineering models for soot formation and deposition. Farmer et al [6] and Jensen [7] developed Level II type models for predicting soot formation and total soot yield from well mixed jet stirred reactors and methane combustion, respectively. The soot nucleation, growth, and oxidation rates were expressed in the form of Arrhenius type rate equations. The effect of local mixing was not included in these models. However, the soot residence time in the combustion chamber was included. The empirical constants were adjusted so that an acceptable fit to available experimental

MODEL LEVEL	APPROACH	EQUATION TYPE	SOLUTION PROCEDURE	APPLICATIONS	ADVANTAGES	DISADVANTAGES
LEVEL I	Correlation of Full Scale Test Data	Single Curve Fit Type Equation	Hand Calculation	Main Chamber Combustion - Seader & Wagner [1] Gas Generator Combustion - Carbon Dep. Program [1]	- Simple Calculation - Correlations based on Gas Generator Test Data	- Not Applicable to New Designs - Qualitative Data for Design Purposes
LEVEL II	1-D Equations Based on Conservation Laws and Models of Physical Processes.	Set of Nonlinear Algebraic Equations Resulting From Direct Integration of the Governing Eqs.	Computer Code	Monopropellant Methane Decomposition - Jensen [7] LO2/RP-1 FRCM [13]	- Engineering Level Model - Model Contains Essential Physics - Easily Implemented on Computer	- Empirical Inputs to Model are Required - Less Accurate as Geometry Becomes More Complex
LEVEL III	Solution of Complete 2-D or 3-D Conservation Equations for Momentum, Mass, Energy, and Soot Concentration Including Combustion Kinetics and Turbulence.	Complex Set of Nonlinear Partial Differential Eqs.	Computer Code	Turbulent Diffusion Flames - Moss [19] Laminar and Turbulent Diffusion Flames - Kennedy et al [20]	- Solution From Governing Equations - Spatial Distributions of Parameters - Applicable to Complex Flow Fields	- Turbulence Closure Problems - Computationally Intensive - Significant Work Required to Program New Code

Figure 4. Modeling Approaches for Low Mixture Ratio Combustion and Carbon Deposition Model

4.2, Model Formulation (cont.)

data was achieved. The basic form of the soot formation and growth equations provides a basis for the development of a Level II Low Mixture Ratio Combustion and Carbon Deposition Model.

The prediction of soot deposition is analogous to chamber heat transfer for which lumped parameter, 1-D models have been proven as adequate design tools once a sufficient amount of experimental verification of empirical constants has occurred. An example of a Level II heat transfer model is the NASA LeRC HOCOOL program for calculating thrust chamber heat transfer with regenerative and film cooling [8]. Correlations for mass transfer coefficients based on local flow properties including the effect of soot particle thermophoresis have been developed by Gokoglu and Rosner [9] and Rosner [10] to predict particle deposition in gas turbines. The net deposition of soot to the wall is ultimately controlled by the adhesion strength of the soot layer versus the shearing action to the high speed flow near the wall. The empirical adhesion strength model for small particles, developed by Zimon [11] and Barengoltz [12] (see Section 4.2.4 for details), is applicable to soot deposits provided the mean adhesion force is known.

Aerojet's Fuel Rich Combustion Model (FRCM) [13] is an example of a Level II type model using a chemical kinetics scheme to calculate the average temperature for fuel rich LOX/RP-1 combustion. This model does not predict soot formation, deposition, or include the effects of mixing processes and chamber geometry. The reaction scheme used in the FRCM could easily be adapted for use in a Level II Low Mixture Ratio Combustion and Carbon Deposition model in order to account for the pyrolysis reactions of LOX/RP-1.

Level III - The Level III models represent the highest level of sophistication and ultimately the most powerful modeling capability. The objective of such models is to predict the formation, growth, and transport of soot throughout the flow field. Detailed kinetic models of soot formation have been studied by several researchers such as Frenklach et al [14]. In general, such reaction schemes (involving on the order of 500 to 1000 equations) have been unsuccessful in predicting soot formation and are computational intensive. The current trend in Level III type modeling uses empirically derived relationships between the local mixture ratio, flow field, and temperature field to the amount of soot formed. An early attempt at this type of modeling was performed by Gore and Faeth [15] for ethylene diffusion flames using an empirical correlation between the soot volume fraction and the local mixture ratio. This correlation was obtained from measurements made in a laminar axisymmetric diffusion flame. The problem with this correlation

4.2, Model Formulation (cont.)

is that it ignores the effect of the soot particle history and residence time in the flame. It also ignores the effect of mixing rates on the soot chemistry.

Magnussen and Hjertager [16] and Magnussen et al [17] incorporated a model for soot formation into an eddy dissipation model for turbulent combustion. They used the kinetic scheme of Tesner et al [18] for soot formation from air/acetylene combustion by calculating the mass of the soot and mean particle number density. The empirical constants were adjusted to give good agreement between the computations and their experiments.

Recently Moss et al [19] proposed a model which incorporates the essential physics i.e., a nucleation rate, a surface growth rate and a burn-out or oxidation rate. Their rate constants were not known and were determined by fitting their model to measurements in a laminar diffusion flame. The model which they propose may be somewhat difficult to implement in to turbulent flow calculations because of the usual closure problems for the chemical source terms in conventional models of reacting flows. Methods tusing transport equations for probability density functions should overcome the turbulent closure problem.

Kennedy et al [20] have recently developed an improved Level III type model which can be easily incorporated into existing turbulent combustion codes. It should be useful for modeling specific tests to define the empirical constants for a Level II type model. In the absence of adequately reduced chemical schemes for soot formation, the approach is to use the available empirical information which laser diagnostic measurements have provided. In addition, this model is based on a satisfactorily accurate numerical scheme which does not add substantially to the already significant computational burden that is faced in predicting practical turbulent flow fields.

In Kennedy's model, the local mixture ratio is the primary quantity which is calculated. The temperature, density, and the gas composition are determined as functions of the local mixture ratio. The local mixture ratio is also used to determine the soot volume fraction indirectly. The soot volume fraction is not a function of the local mixture ratio, but rather the rates of nucleation, surface growth, and oxidation are functions of local mixture ratio. The conservation equation for the soot volume fraction, ϕ , is then

$$\rho u \frac{\partial \phi}{\partial x} + \rho(v + v_T) \frac{\partial \phi}{\partial y} = \frac{1}{r} \left(\frac{\partial}{\partial r} \left(r \rho D_s \frac{\partial \phi}{\partial r} \right) \right) + \rho w_n + \rho w_g - \rho w_o \quad (1)$$

4.2, Model Formulation (cont.)

where w_n , w_g , and w_o are the rates of soot volume formed by nucleation, surface growth, and removed by oxidation respectively. A thermophoretic radial velocity, v_T , of soot particles is included and is very important in determining soot deposition rates. This model has been used successfully to predict soot formation and transport in laminar and turbulent flames.

4.2.1 Overall Methodology

The model chosen for development in this program was the near-term, tractable model (i.e. Level II model) consisting of an empirically based 1-dimensional representation of the gas generator combustion and flow. The essential elements of the model are (1) combustion kinetics submodel, (2) soot formation submodel, (3) 1-D flow model, and (4) a soot formation model. The outputs of the model are axial profiles of temperature, gas composition, soot yield, pressure, wall shear stress, wall thermal resistance, deposit thickness, and deposition rate. The elements of the model are illustrated Figure 5. The basic inputs to the model are propellant type, a mixing parameter characterizing the injector, flowrate, mixture ratio, chamber pressure, and chamber geometry. From these inputs, a soot formation model calculates the soot particle nucleation and growth rates. The concentration of combustion products and bulk temperature are provided by a kinetic model consisting of a reduced set of gas phase combustion and pyrolysis reactions. The soot formation model is iterated with a 1-D flow model to determine the amount of soot (soot volume fraction), bulk temperature, and wall shear stress down the length of the chamber.

In this model, the soot formation process is decoupled from the deposition process, except to the extent that soot build up over time may cause an increase in chamber pressure. Therefore, once the flow conditions and soot volume fraction profile have been specified down the length of the chamber, the deposition model is used to predict the thickness of the soot deposit. The input to this part of the model is the wall shear stress, soot volume fraction, and wall temperature at specified stations down the length of the gas generator. The soot deposition at each station is calculated in two steps. First, a mass transfer coefficient for soot is used to calculate the maximum possible deposition. The net deposition is then determined by calculating a "sticking fraction" of soot on the wall by comparing the soot layer adhesion strength to the wall shear stress.

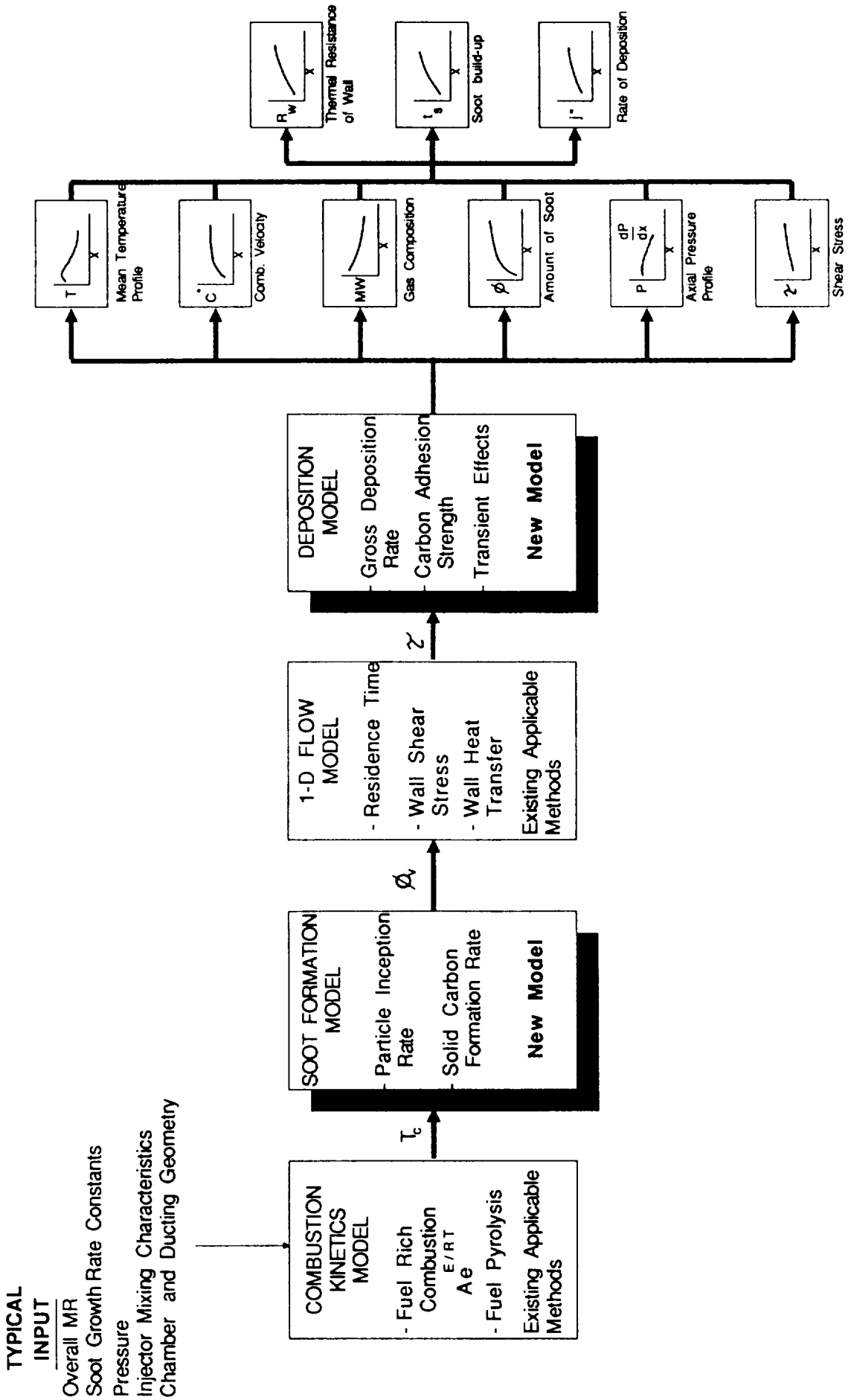


Figure 5. Elements of the Low Mixture Ratio Combustion and Carbon Deposition Model

4.2, Model Formulation (cont.)

Models currently exist for the chemical kinetics and 1-D flow which are directly applicable with only slight modification. The kinetics submodel is used to predict only combustion temperature, but not soot nucleation. Therefore, the kinetics model can be replaced with empirical data at this level of modeling. The emphasis during this program was placed on formulating the basic equations of the soot formation and deposition models.

4.2.2 Identification of Model Parameters

From the results of the literature review key parameters affecting soot formation and deposition at low mixture ratio conditions have been identified. An initial screening of the effects of combustion parameters on soot formation and deposition was conducted in the first phase of the program and was presented in Reference [1]. That database has been extended to include candidate parameters for the model. The results of this review are the parameters which have been incorporated into the models for combustion, soot formation, and deposition. A summary of key parameters is shown in Figure 6 where the effect on soot formation and deposition is indicated.

4.2.3 Soot Formation Model

A soot formation model has been derived which accounts for the contribution of the inception rate of small (1-10 nm diameter) soot particle nuclei and growth/coagulation of the particles as they traverse the gas generator. Because the soot particle inception rate is one of the slowest reactions relative to gas phase combustion reactions, it is very sensitive to fluid mechanics (i.e. mixing characteristics) of the fuel and oxidizer. Figure 7 illustrates the potential effect of mixing (in terms of a relative velocity gradient between spray fans) on particle formation rate. The data shown on the figure were obtained in a counter flow diffusion flame where the mixing rate was precisely controlled [24]. At sufficiently high mixing rates, there is insufficient time for soot particles to form (nucleate) and the overall soot formation is suppressed. The soot particle number density at inception drops from a typical value of 10^{15} particles/cm³ very rapidly to nearly zero. At low mixing rates, well below that sufficient to cause soot suppression, the dominate processes affecting soot formation are the soot surface growth reactions and residence time of soot particles in hot regions of the flow. Under these conditions, total soot yield is relatively insensitive to the precise number density (i.e. variations of a factor to 10 to 100) at formation because the rapid coagulation and growth of "young" soot particles controls the surface area available for the addition of solid mass to the particle. The empirical model which has been derived to account for these

PARAMETER	ANALYTICAL VARIABLE	EXPRESSION	EFFECT ON SOOT FORMATION	EFFECT ON SOOT DEPOSITION	REFERENCE
Fuel Type	Carbon/Hydrogen Ratio	$C_n H_m$	Generally Higher Soot Loading From Heavier Hydrocarbons	Physical Appearance and Texture Differences - no quantitative trends	Carbon Deposition Program [1]
Chamber Pc	—	P_c	Increases as P from 1 to 10 atm. Little data at high pressures.	Slight increase in Deposition as Pressure is Increased	Flower [19], Carbon Deposition Program [1]
Carbon/Oxygen Ratio	Mixture Ratio	$\frac{W_{O_2}}{W_{fuel}}$	Increase with increasing mixture ratio for 0.25 <MR <1.0 and then decreases	Effect Unknown	Carbon Deposition Program [1] Photographic Comb. [22]
Residence Time	—	$t = \frac{\rho_{loc} A}{W_{tot}}$	Soot formation increases with increasing residence time	No Effect	Farmer [6] Prado [23]
Mixing Rate	Scalar Dissipation Rate	$\bar{\chi} = 2D(\nabla \xi)^2$	Suppression of Soot particles nucleation at high values of scalar dissipation rate	No Effect	Kennedy [24]
Turbulence	Turbulence Intensity	$\frac{u'_i}{\bar{u}_i}$	Increased turbulence intensity increases mixing and should reduce soot formation	Increased turbulent transport increases deposition	Niel & Kennedy [25]
Pressure Gradient	—	$\frac{dp}{dx}$	Favorable pressure gradients cause increased mixing and reduces soot	No Direct Effect	Niel & Kennedy [25]
Spray Atomization	Mean Diameter	d_{SMD}	Larger droplets increase vaporization time, increasing coking and reducing mixing	Increased Coking increases oily residue deposits	Eckerle and Rosjford [26]
Wall Temp.	Ratio of Wall Temp to Freestream Gas Temperature	$\frac{T_w}{T_e}$	No Effect	Thermophoretic deposition increases as wall temperature ratio decreases	Rosner [4] Gokoglu & Rosner [9] Talbot [5]
Soot Deposit Adhesion Strength	Mean Adhesion Strength	$K_{50\%}$	No Effect	Major effect, controls final amount of soot deposited out on surface	Zimon [11] Barengoltz [12]

Figure 6. Parameters Affecting Soot Formation and Deposition

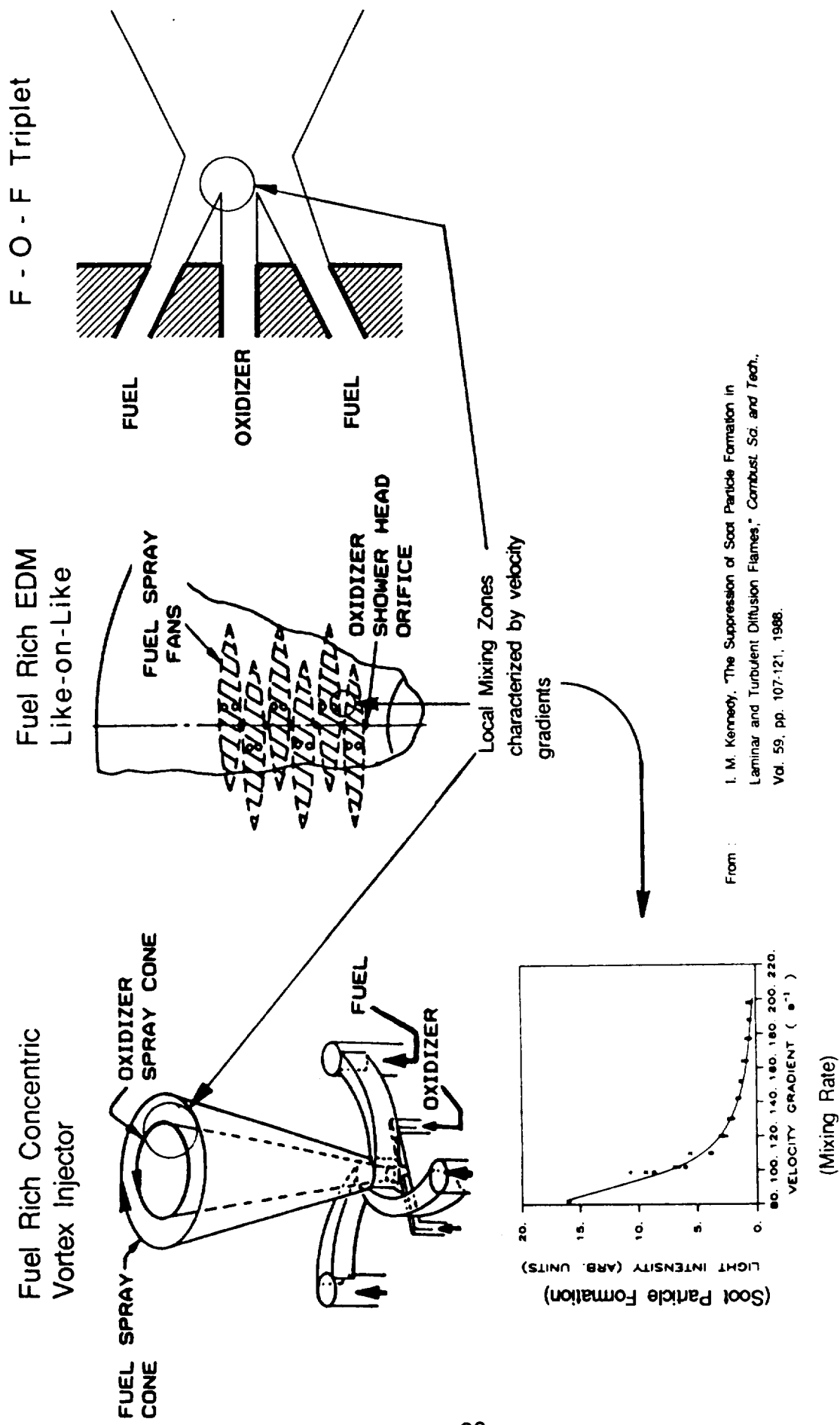


Figure 7. High Injector Mixing Rates May Suppress Soot Particle Formation

4.2, Model Formulation (cont.)

processes uses measured values for the particle inception rate and the soot surface growth rate for particular hydrocarbon fuels. The derivation of the model is described below .

First, the effect of soot surface growth reaction (i.e. the conversion of gas phase hydrocarbons to soot) is derived. The soot volume fraction is defined as the volume of soot per unit volume of flow as given by eq.2.

$$\phi_v = N \frac{\pi}{6} d_p^3 \quad (2)$$

N = Soot particle Number Density {particles/cm³}

d_p = Soot Particle Diameter

The effect of the surface growth reactions is to increase the mass and therefore the volume of soot. The change in mass as a function of time is therefore:

$$\frac{dm}{dt} = N \pi d_p^2 C \rho_s \quad (3)$$

C = Soot Surface Growth Rate

ρ_s = density of soot particle = 1.9 gm/cm³

The soot surface growth rate, C , represents an average of all the reactions causing growth of soot as shown by eqs. 4 and 5.



$$k = \rho_s C = \rho_s a \left(\frac{c}{o} \right)^n \exp \left\{ \frac{E_a}{R} \left(\frac{1}{T_{ref}} - \frac{1}{T_c} \right) \right\} \quad (5)$$

where: a = rate constant

c/o = local carbon to oxygen ratio

4.2, Model Formulation (cont.)

E_a = activation energy

T_c = bulk gas temperature

T_{ref} = reference temperature

An overall rate is used in the model because of a lack of detailed kinetics models. This overall reaction rate can be directly measured with the fuels of interest in controlled combustion experiments. The soot surface growth rates for hydrocarbon/air diffusion and premixed flames have been measured and for a given fuel, a single step rate equation such as eq. 5 has proven valid over a wide range of mixture ratios [27].

Substituting for d_p in eq. 3 with eq. 2 and dividing by ρ_s , the rate of change of the soot volume fraction as a function of time is obtained in eq. 6.

$$\frac{d\phi}{dt} = (\pi N)^{1/3} (6\phi)^{2/3} C \quad (6)$$

Next, the effect of soot particle coagulation which changes the soot particle number density in time, $N(t)$, must be derived. Following the derivation of Hinds [28], first the diffusion of particles to a single particle is considered and then extended to all the particles in the unit volume. For an individual particle the rate of collisions per unit time per unit area is governed by Fick's law of diffusion (eq. 7.)

$$J = -D \frac{dN}{dx} \quad (7)$$

D = Diffusion Coefficient

J = Flux of particles to the surface

The collision surface is assumed to be twice the soot particle diameter. The rate of collisions between the selected particles and the surrounding particles as a function of time is equal to the product of the collision surface area and the flux of particles.

$$\frac{dn}{dt} = 4\pi d_p^2 D \frac{dN}{dx} \quad (8)$$

n = number of collisions

4.2, Model Formulation (cont.)

The concentration gradient at the surface is obtained by solving eq. 7.

$$\frac{dN}{dx} = \frac{-2N}{d_p} \quad (9)$$

The rate of collisions for all the particles is equal to $N/2$ times the rate of a single particle. (The factor of 2 prevents double counting of collisions.) The rate of collisions per unit volume is:

$$\frac{dn_c}{dt} = 4\pi d_p D N^2 \quad (10)$$

n_c = collisions per unit volume

Assuming that for each collision of a soot particle there is a reduction of one in the number of particles in a unit volume, the number concentration is reduced by one. The change in number concentration is exactly equal to the collision rate as shown in eq. 11.

$$\frac{dN}{dt} = -\frac{dn_c}{dt} \quad (11)$$

For the size range of soot particles, 10 to 200 nm diameter, the product $d_p D$ is nearly constant, therefore, the time rate of change of the number concentration is eq. 12.

$$\frac{dN}{dt} = -\beta N^2 \quad (12)$$

where $\beta = 4\pi d_p D$

The term, β , is called the particle collision coefficient. The particle number density as a function of time is obtained by integrating eq. 12, assuming an initial particle number density at formation of N_o .

$$N(t) = \frac{N_o}{1 + \beta N_o t} \quad (13)$$

An expression for the soot volume fraction as a function of time (or location in the gas generator) can be derived by substituting eq. 13 into eq. 6 and integrating. The resulting expression is:

4.2, Model Formulation (cont.)

$$\phi_s(t) = \left[\left(\frac{V_p}{N_p} N_o \right)^{1/3} + \frac{C}{\beta N_o^{2/3}} \left\{ (N_o \beta t + 1)^{2/3} - 1 \right\} \right]^3 \quad (14)$$

Equation 14 provides a means of calculating the axial distribution of soot in the gas generator. The primary variables in the model are the number density of particles at inception, N_o (from the particle inception rate), the soot surface growth rate, C , and the particle collision rate, β . The first two of these variables are quantities which will eventually have to be anchored experimentally. The collision rate of soot particles can be calculated from existing theory and is essentially independent of fuel type. The effect of pressure and temperature are contained in the soot surface growth rate term. As the flow mixes and the the temperature of the gas becomes uniform the surface growth reactions stop and the soot volume fraction becomes a constant. The effect of mixing is contained in the number density at particle inception, N_o , as discussed above.

For the one dimensional streamtube model approach, all parameters are represented by bulk, average values. If the propellants are injected premixed, then the one-dimensional model provides a very good approximation for the flow. Discrete and separate injection of the fuel and oxidizer adds two features, mixing and local temperature variations, which are very important for predicting soot formation. The first feature, mixing, affects the soot particle inception rate. The second feature, local temperature variations in the flow, provide high temperature regions where soot particles can grow. Each of these features impacts the total amount of fuel converted solid carbon. In order to account for these processes in the model, empirical correlations for the particle number density at nucleation, N_o , and the "effective" combustion temperature used in eq. 5, based on the injector mixing efficiency, ϵ_m , must be developed. The basis for the correlation is the assumption that a high mixing efficiency that is achieved in a short time (or short chamber length) implies rapid fuel and oxidizer mixing and the "effective" combustion temperature must quickly approach the bulk temperature. Sufficient data does not exist to quantitatively define this correlation, however, the proposed form of this correlation is given in eq. 15.

$$N_o = \epsilon_m(x) \cdot \frac{x}{v} \cdot K_1 \cdot \exp\left(-c_1 \frac{x}{L}\right) \quad (15)$$

where: $\epsilon_m(x)$ = axial mixing efficiency profile

v = average velocity

4.2, Model Formulation (cont.)

L = chamber length

The "effective" combustion temperature is then related to the bulk temperature by a correlation of the form in equation 16.

$$T_c = T_{bulk} \cdot \frac{K_2}{\epsilon_m(x)} \quad (16)$$

where: T_{bulk} = Average Temperature from kinetic model

The mixing efficiency can be input from experimental data or calculated for conventional injector element configurations using the standard JANNAF performance prediction methodology [29]. The empirical constants appearing in eqs. 17 and 18, K_1 , K_2 , and c_1 , can be anchored for different injector designs by measurements for the soot particle size and soot volume fraction at several axial positions in a prototype gas generator. Details of the measurement techniques and test requirements are described in Section 4.4.

The model has been used with the 1986 LO₂/propane tests as test cases. Table I contains a summary of the LO₂/propane Task V data together with the calculation of the soot volume fraction (ϕ) for each test. The calculation was made assuming a soot surface growth rate of

$$C = 5.0e - 07(C/O)^2 e^{\left(\frac{E_a}{R} \left(\frac{1}{T_{ref}} - \frac{1}{T_c}\right)\right)}$$

$$E_a = 20 \frac{\text{kcal}}{\text{mole}}$$

$$T_{ref} = 1700\text{K}$$

which is typical for premixed hydrocarbon/air combustion systems with C₂ or C₃ type fuels. A average particle collision rate was calculated for 0.1 micron soot particles at MR= 0.35, 1000 psia and T_c=1400 F. The purpose of these calculations is to see if the proposed model exhibits the same trends as those observed in the testing. There is no way to infer the value of the soot volume fraction directly from the Task V data.

Figure 8 shows the calculated soot volume fraction as a function of mixture ratio. In general the soot volume fraction in the range of interest (M.R. 0.3 to 0.5) is very sensitive to mixture ratio. Scatter in the data is due to the fact that the final soot volume fraction is dependant on residence time in the gas generator. The absolute value of the soot volume fraction

TABLE I. Calculation Of Soot Volume Fraction For Task V LO₂/Propane Tests

TEST NO.	P _c psia	MR	W _{tot} lbm/s	W _{fuel} lbm/s	W _{ox} lbm/s	C/O	T _c F	DENSITY F lbm/ft ³	t _{res} sec	N _o m ⁻³	Beta cm ³ /s	C	Phi
113	1036	0.26	2.04	1.62	0.42	4.19	1080	1.54	0.0305	1.00E+18	8.00E-10	3.72E-09	1.58E-08
114	1065	0.35	1.90	1.41	0.49	3.11	1380	1.32	0.0282	1.00E+18	8.00E-10	1.93E-08	5.01E-07
120	1219	0.44	1.59	1.10	0.49	2.47	1900	1.18	0.0301	1.00E+18	8.00E-10	1.05E-07	5.84E-05
125	1020	0.29	1.95	1.51	0.44	3.75	1200	1.40	0.0292	1.00E+18	8.00E-10	7.61E-09	5.81E-08
126	1061	0.41	1.50	1.06	0.44	2.66	1600	1.18	0.0318	1.00E+18	8.00E-10	3.16E-08	2.07E-06
128	873	0.39	1.17	0.84	0.33	2.79	1550	0.99	0.0344	1.00E+18	8.00E-10	1.59E-08	3.64E-07
129	866	0.33	1.43	1.08	0.35	3.30	1280	1.14	0.0322	1.00E+18	8.00E-10	6.37E-09	4.31E-08
130	820	0.34	1.30	0.97	0.33	3.20	1350	1.03	0.0323	1.00E+18	8.00E-10	7.77E-09	6.51E-08
131	1473	0.29	1.55	1.20	0.35	3.75	1380	1.83	0.0478	1.00E+18	8.00E-10	1.40E-08	3.52E-07
132	1484	0.33	1.40	1.05	0.35	3.30	1300	1.92	0.0558	1.00E+18	8.00E-10	6.88E-09	7.42E-08
133	1497	0.38	1.17	0.85	0.32	2.87	1500	1.74	0.0604	1.00E+18	8.00E-10	1.28E-08	3.40E-07
134	1561	0.39	2.05	1.47	0.58	2.79	1720	1.63	0.0323	1.00E+18	8.00E-10	9.88E-08	5.30E-05

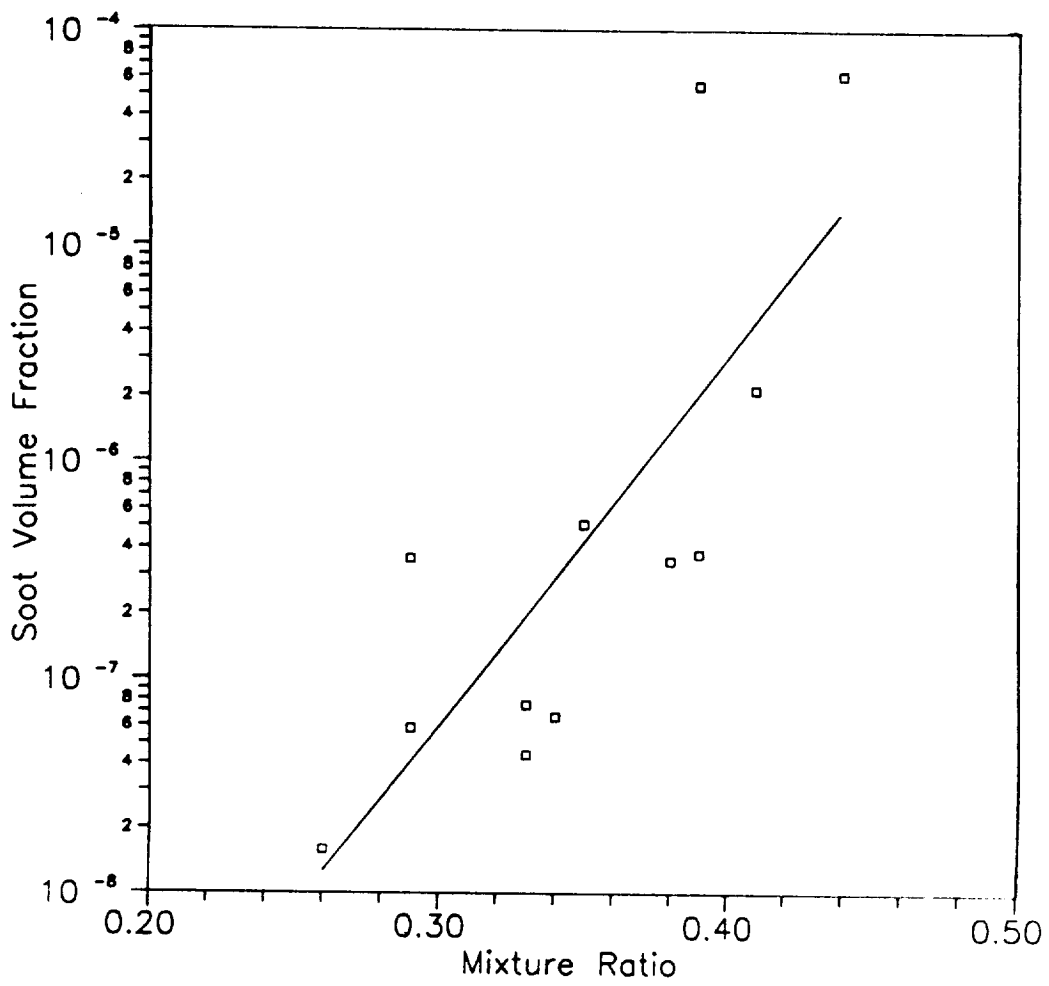


**Figure 8. Prediction of Soot Volume Fraction for Task V
LO₂/Propane Tests**

4.2, Model Formulation (cont.)

appears to be of the correct order of magnitude. Sooting flames typically exhibit soot volume fractions ranging from $1.0\text{e-}07$ to $1.0\text{e-}05$. Inspection of Figure 8 shows over an order of magnitude increase in the soot volume fraction between $\text{MR}=0.30$ and $\text{MR}=0.40$. This increase correlates to the measured increase in pressure drop across the turbine simulator during testing as shown in Figure 9. The soot deposition rate is directly proportional to the soot volume fraction, therefore a large increase in soot production is expected to produce large change in the indicated deposition.

4.2.4 Soot Deposition Model

The net soot deposition is the difference between the gross deposition rate and the removal (reentrainment) rate. To obtain the gross deposition rate, anchored heat transfer coefficients are used to calculate mass transfer coefficients. The mass transfer coefficients are then modified to account for thermophoresis ("mass transfer down a temperature gradient.") The effect of thermophoresis on soot deposition is similar to that of wall suction on heat transfer. For soot particles which range in size from 10 to 200 nm, deposition via thermophoresis is several orders of magnitude greater than diffusion or inertial impaction. The removal rate is determined separately from the flow conditions at the wall. The soot removal rate is determined from a balance of the strength of the soot particle adhesion to the wall versus the fluid shear stress at the wall.

The gross thermophoretic deposition is calculated using the correlation proposed by Rosner et al [4,20]. This correlation is based on the assumption that the thermophoretically enhanced deposition of soot is proportional to the "normal" (i.e. diffusion only) mass transfer coefficients, as shown in eq. 17,

$$\dot{j}_{\text{deposit}} = \rho v \phi_e \text{St}_m f_1(B) f_2(D) \quad (17)$$

where the normal Stanton number for mass transfer is defined in eq. 18.

$$\text{St}_m = \frac{j''}{\rho v} \quad (18)$$

The first function in eq. 17, $f_1(B)$, accounts for the transport of soot to the wall due to the overall temperature gradient, which is analogous to "wall suction" on heat transfer. The second function, $f_2(D)$, accounts for the fact that the temperature gradient is not linear, and has a nonzero second derivative. The effect of a nonlinear second derivative is that the wall acts like a sink for soot particles due to a thermophoretic acceleration of particles towards the wall. Based on laminar deposi-

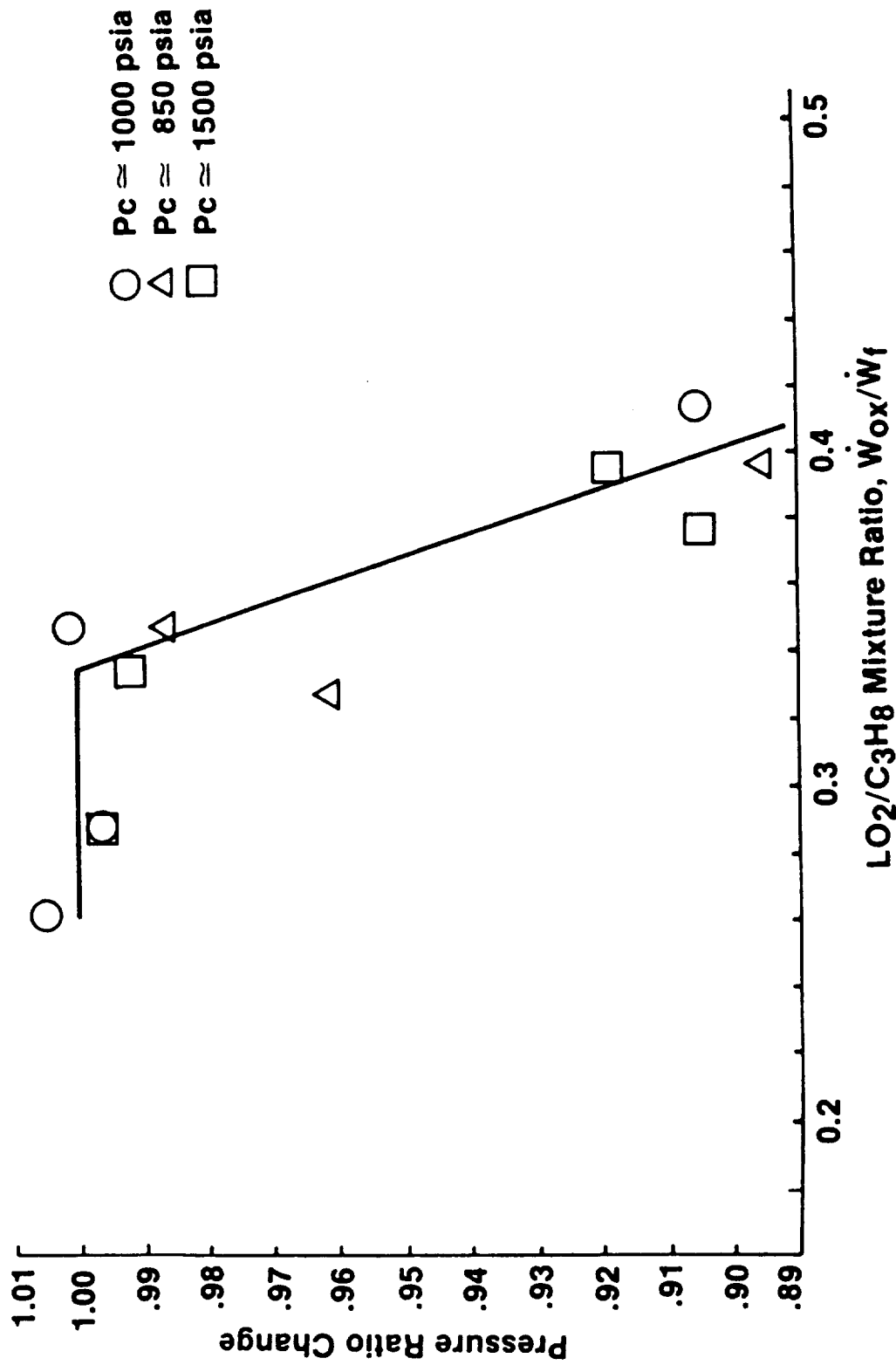


Figure 9. Pressure Drop Due to Carbon Deposition Measured During Task V

4.2, Model Formulation (cont.)

tion measurements and correlation with turbulent flow CFD calculations the functional form of the relations has been found by Rosner [4] to be as shown in eqs. 19 and 20.

$$f_1(B) = \left(\frac{-B}{1 - e^B} \right) \quad (19)$$

$$f_2(D) = e^{-D} \quad (20)$$

The variables B and D are defined by eqs. 21 and 22,

$$B = -(0.55Le)_w \frac{St_h}{St_m} \left(\frac{T_g - T_w}{T_w} \right) \quad (21)$$

$$D = (0.55Le)_w \left(\frac{T_g - T_w}{T_w} \right) \quad (22)$$

where: T_g = bulk gas temperature

T_w = local wall temperature

where, the Stanton number for heat transfer, St_h , and the Lewis number, Le , are defined based on bulk property data as shown in eqs. 23 and 24.

$$St_h = \frac{Nu}{RePr}, \quad Nu = \frac{hd}{k} \quad (23)$$

where:

$$Re = \frac{4\dot{w}_{tot}}{\pi d \mu}, \quad Pr = \frac{\mu C_p}{k}$$

h = local heat transfer coefficient

k = bulk gas thermal conductivity

C_p = bulk gas specific heat

μ = bulk gas viscosity

$$Le = \frac{\mu}{\rho D} \quad (24)$$

4.2, Model Formulation (cont.)

The local Nusselt number, Nu , can be readily obtained from existing heat transfer correlations or derived from combustion chamber heat flux data such as that obtained during the Task V testing. Finally the gross deposition rate can be expressed as shown in eq. 25.:

$$j_{deposit}'' = \phi_e \rho v St_m \left(\frac{-B}{1 - e^B} \right) e^{-D} \quad (25)$$

The deposition rate calculated from eq. 25 assumes that all the soot deposited on the surface remains there. In order to determine the actual deposition, the effect of reentrainment of deposited soot into the gas stream must be considered. The net deposition rate is obtained by multiplying the gross deposition rate by a "sticking fraction" that varies between 0 and 1. No theoretical models of soot particle adhesion strength were found in the literature. Some of the forces responsible for the adhesion of soot to a solid surface include contact potential, electrostatic, van der Waal's and capillary forces [11]. In the absence of a theoretical treatment of the soot adhesion strength, the "sticking fraction" is based on assuming a known statistical distribution for the adhesion strength of a soot particle to a wall. A log normal type distribution based on the dust particle adhesion work of Berengoltz [12] has been found to also characterize soot particle adhesion by Makel and Kennedy [30]. In addition, the primary force causing reentrainment and reducing deposition has been determined to be the fluid shear stress at the wall [30,31]. Therefore, the "sticking fraction" of soot particles is the percentage of particles with adhesion strengths greater than the mean fluid shear stress (or alternatively the probability that a given soot particle has an adhesion strength greater than the mean shear stress at the wall).

The adhesion force, F_{ad} , for particles is assumed to be proportional to particle diameter, d_p , as in eq. 26

$$F_{ad} = k d_p^2 \quad (26)$$

and distributed according to a log-normal distribution in k . The characteristic force is $F_{50\%}$ which corresponds to the force required to remove 50% of the deposited particles. The "sticking fraction" is defined as one minus the probability that the surface shear stress, τ , exceeds the adhesion force, F_{ad} , as given in eq. 27.

4.2, Model Formulation (cont.)

$$R = P(\tau \geq F_{ad}) = \frac{1}{\sqrt{2\pi}} \int_{-\infty}^{(\ln \kappa^* - m)/\sigma} \exp\left(\frac{-k^2}{2}\right) dk \quad (27)$$

where: $\kappa^* = \tau/d_p^2$
 $m = \ln(\kappa_{50\%})$
 $\sigma = \text{standard deviation}$

The net particle deposition can then be expressed as eq. 28.

$$j_{net} = (1 - R)\phi_e \rho v St_m \left(\frac{-B}{1 - e^B}\right) e^{-D} \quad (28)$$

The Task V test data can not be used to verify the deposition model. The turbine simulator flow blockage tests yield the percent reduction of $C_d A$ (product of the discharge coefficient and available flow area.) In the absence of post-test physical measurements of the flow area, the only way to relate the pressure drop data to deposit thickness is to assume that the discharge coefficient is constant. Inspection of post test hardware photographs indicates dramatic changes in the shape and roughness of flow passages, indicating that very large variations in C_d are to be expected. In addition, the deposition model requires input of the free stream soot volume fraction and the adhesion strength distribution.

Figures 10 and 11 show the parametric behavior of the deposition model at representative gas generator conditions. The conditions chosen were:

$$\begin{aligned} P_c &= 1000 \text{ psia} \\ T_b &= 1520 \text{ F} \\ \phi_e &= 0.0001, 0.00005, 0.000025 \end{aligned}$$

The figures indicate two major flow effects on soot deposition. Figure 10 shows the increase in deposition mass flux as the flow velocity is increased in various size nozzles. The calculations assume a perfectly adherent wall (i.e. $R=0$). The deposition is proportional to the free stream soot volume fraction, ϕ_e , and approximately linear with velocity (the square of the nozzle diameter).

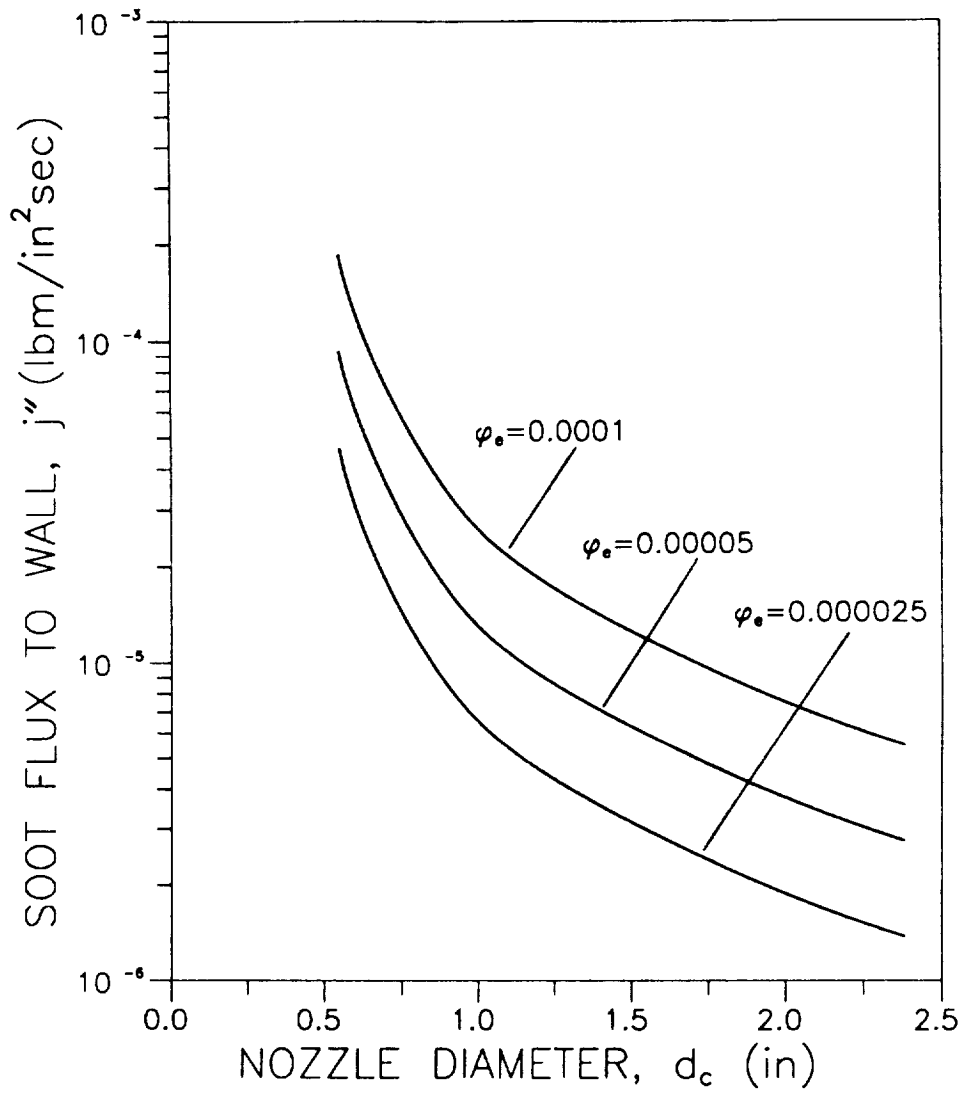
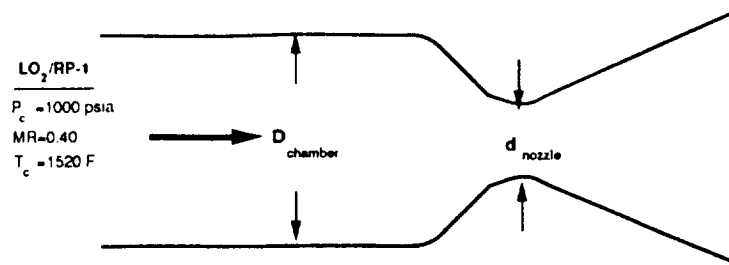


Figure 10. Prediction of Carbon Deposition as a Function of Turbine Inlet Nozzle Diameter for Constant Flowrate of 2.0 lbm/sec

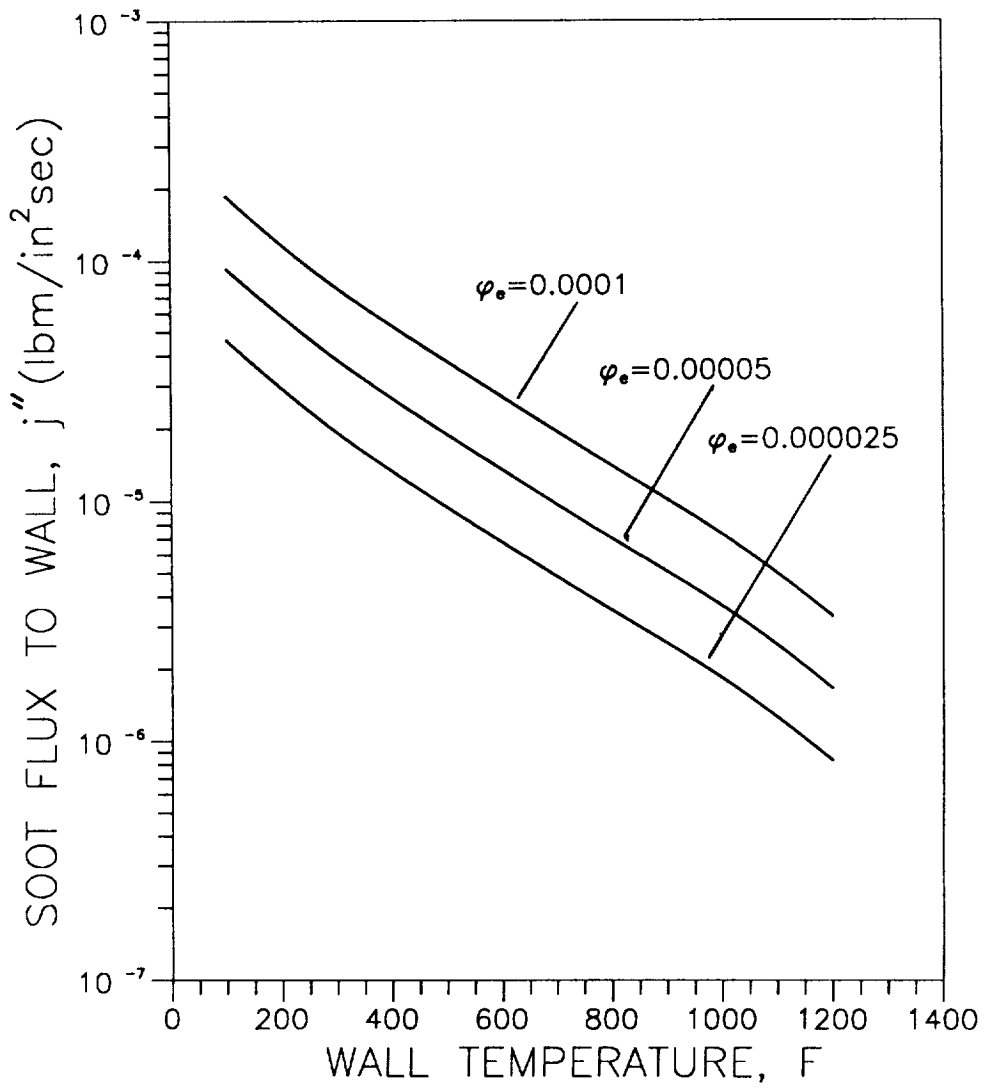


Figure 11. Predicted Effect of Wall Temperature on Carbon Deposition for Gas Temperature of 1520 F in a 20:1 Contraction Ratio Nozzle with LO₂/RP-1 at MR=0.4 and 2 lbm/sec.

4.2, Model Formulation (cont.)

Figure 11 shows the effect of thermophoresis on deposition. As the wall temperature is increased towards the free stream temperature the deposition rate can vary by two orders of magnitude.

4.2.5 1-D Flow Model

The 1-D flow model is used (1) to convert the time variable in the soot volume fraction equation (eq. 14) to an axial position, (2) to calculate the axial pressure profile, and (3) to include the effect of various hardware geometries. The model assumes a 1-D isentropic flow, with temperature dependent properties and an multiconstituent flow. The equations for this type of model are well known [32] and are repeated here for completeness. The principle relations are mass continuity, conservation of momentum, and conservation of energy as listed in eqs. 29, 30, and 31.

$$\frac{d}{dx}(\rho_i v \bar{a}) = \omega_i r^* \bar{a} \quad (29)$$

where: ρ_i = density of *i*th species
 ω_i = species production rate
 \bar{a} = cross sectional area
 r^* = throat radius
 x = normalized axial distance
 v = axial velocity

$$\rho v \frac{dv}{dx} + \frac{dP}{dx} = 0 \quad (30)$$

$$h + \frac{1}{2}v^2 = H_c \quad (31)$$

Using constituent relations for the system enthalpy, pressure, and multi-species gas constant (eqs. 32, 33, and 34)

$$h_i = \int_0^T C_{p_i} dT + h_{i_0} \quad (32)$$

4.2, Model Formulation (cont.)

$$P_i = \rho_i R_i T \quad (33)$$

$$R = \sum_{i=1} c_i R_i \quad (34)$$

the equations can be derived in terms of the gas generator geometry area variation, where the axial position and area have been normalized by the throat radius, as listed in eqs 35 through 40.

$$\frac{dc_i}{dx} = \frac{\omega_i r^*}{\rho v} \quad (35)$$

$$\frac{dv}{dx} = \left[\frac{1}{\bar{a}} \frac{d\bar{a}}{dx} - A \right] \frac{v}{M^2 - 1} \quad (36)$$

$$\frac{dr}{dx} = - \left\{ \left[\frac{1}{\bar{a}} \frac{d\bar{a}}{dx} - A \right] \frac{M^2}{M^2 - 1} + A \right\} \rho \quad (37)$$

$$\frac{dT}{dx} = - \left\{ \left[\frac{1}{\bar{a}} \frac{d\bar{a}}{dx} - A \right] \frac{(\gamma - 1)M^2}{M^2 - 1} + B \right\} T \quad (38)$$

$$B = \frac{(\gamma - 1)}{\gamma} \frac{r^*}{P v} \sum_{i=1} \omega_i h_i \quad (39)$$

$$M = \frac{v}{\sqrt{\gamma RT}} \quad (40)$$

Once the bulk flow has been calculated the axial wall shear stress can be approximated by existing correlations based on the flow Reynolds number [33] or by 2-D boundary layer calculation using JANNAF boundary layer codes such as BLIMP-J [34] and Boundary Layer Module[32].

4.2.6 Combustion Kinetics Model

In order to calculate the mean axial temperature profile in the gas generator, either test data or a chemical kinetics model for the low MR combustion must be used. Simplified combustion kinetics models for LO₂/RP-1 such as the Fuel Rich Combustion Model [13] have

4.2, Model Formulation (cont.)

proven adequate for predicting combustion temperature but have not successfully predicted soot particle inception and coagulation. For propane, several potential reaction schemes exist which should be useful in constructing a kinetics reaction scheme [35]. The completed version of the model will use a kinetics model such as the FRCM or a variant. The reaction rates will be expressed in terms of modified Arrhenius rate expression for j reactions such as eq. 41.

$$k_j = a_j T^n e^{(-E_a/RT)} \quad (41)$$

The resulting set of equations are a coupled set of nonlinear ordinary differential equations which can be integrated in time with the 1-D flow equations to provide the energy release and temperature profile in the gas generator.

The FRCM starts by assuming that all the oxidizer reacts with a portion of the fuel to produce equilibrium combustion products. The JANNAF One-Dimensional Equilibrium (ODE) computer program is used to determine the combustion products. The remainder of the fuel is presumed to vaporize and react kinetically with the ODE predicted combustion products. The JANNAF One-Dimensional Kinetics (ODK) computer program is used for the kinetics calculation. The fuel vaporization is modeled using a temperature dependent rate expression to permit its use in the the ODK program. The vaporized fuel then undergoes kinetically limited combustion to form the final products. While this approach is not a true representation of the combustion presumed occurring in the gas generator, sufficient adjustment of rate constants and activation energies has yielded a reaction set which shows good agreement with RP-1 test data [1].

4.3 INJECTOR MIXING EXPERIMENTS

Cold flow tests were conducted to assess whether typical gas generator combustion is diffusion flame-like (mixing limited) or premixed (kinetically limited) relative to typical soot formation rates. The tests were conducted using the high injection density injector (Figure 12). Air was used to simulate the oxygen and Freon 116 was used to simulate the fuel. The tests were conducted at the Combustion Research Laboratory at the University of California at Davis. The mixing was visualized by imaging the laser light scattered off fuel and oxidizer molecules. The Rayleigh scattered light was from a laser sheet passed through the flow and perpendicular to the injector face. The propellant simulants were introduced as gases with mixture ratios of 0.25 to 0.5 and injection momentum ratios comparable to the Task V test conditions. Because the propellants were injected as gases, mixing occurs faster than with cold (i.e. below the critical temperature)

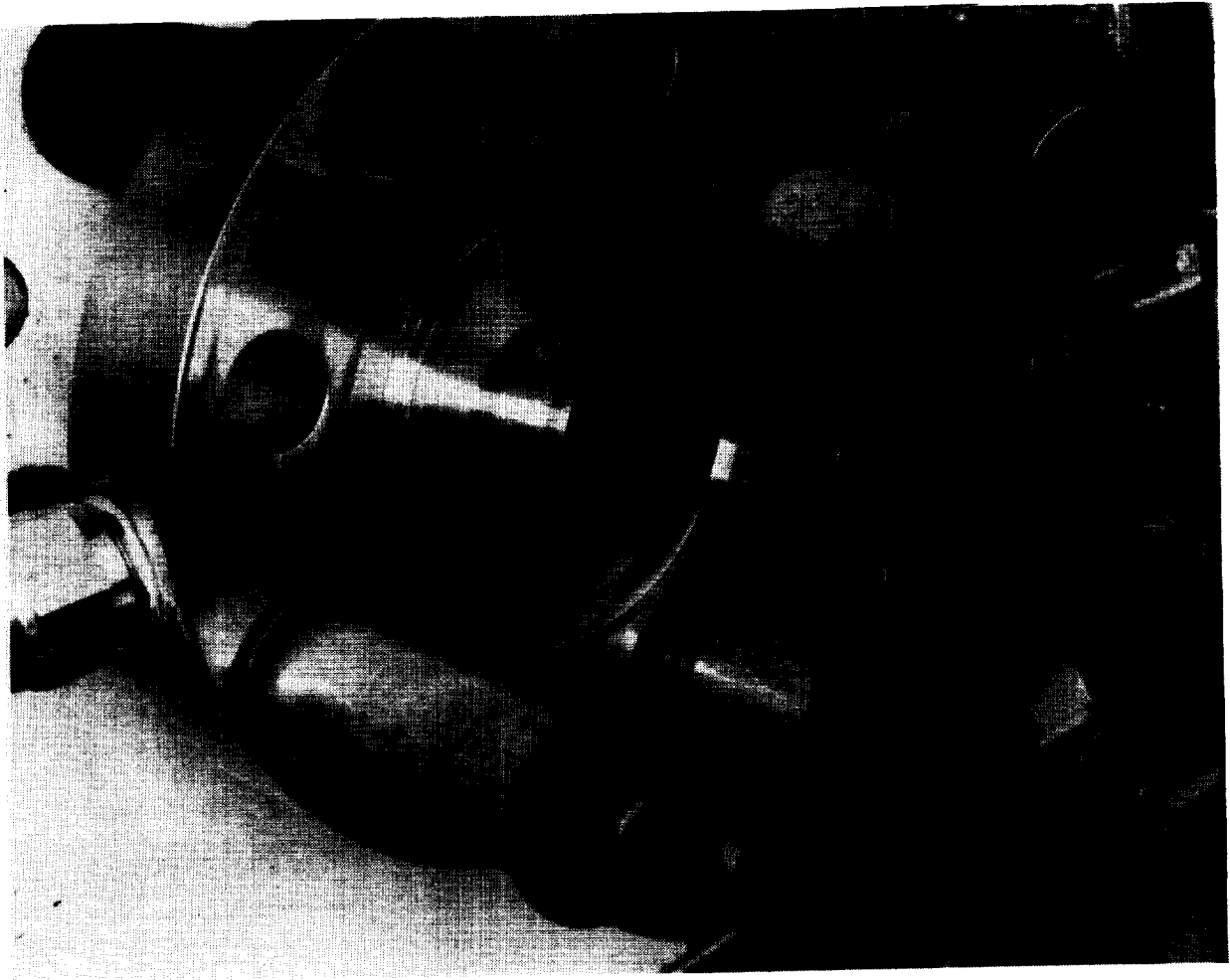
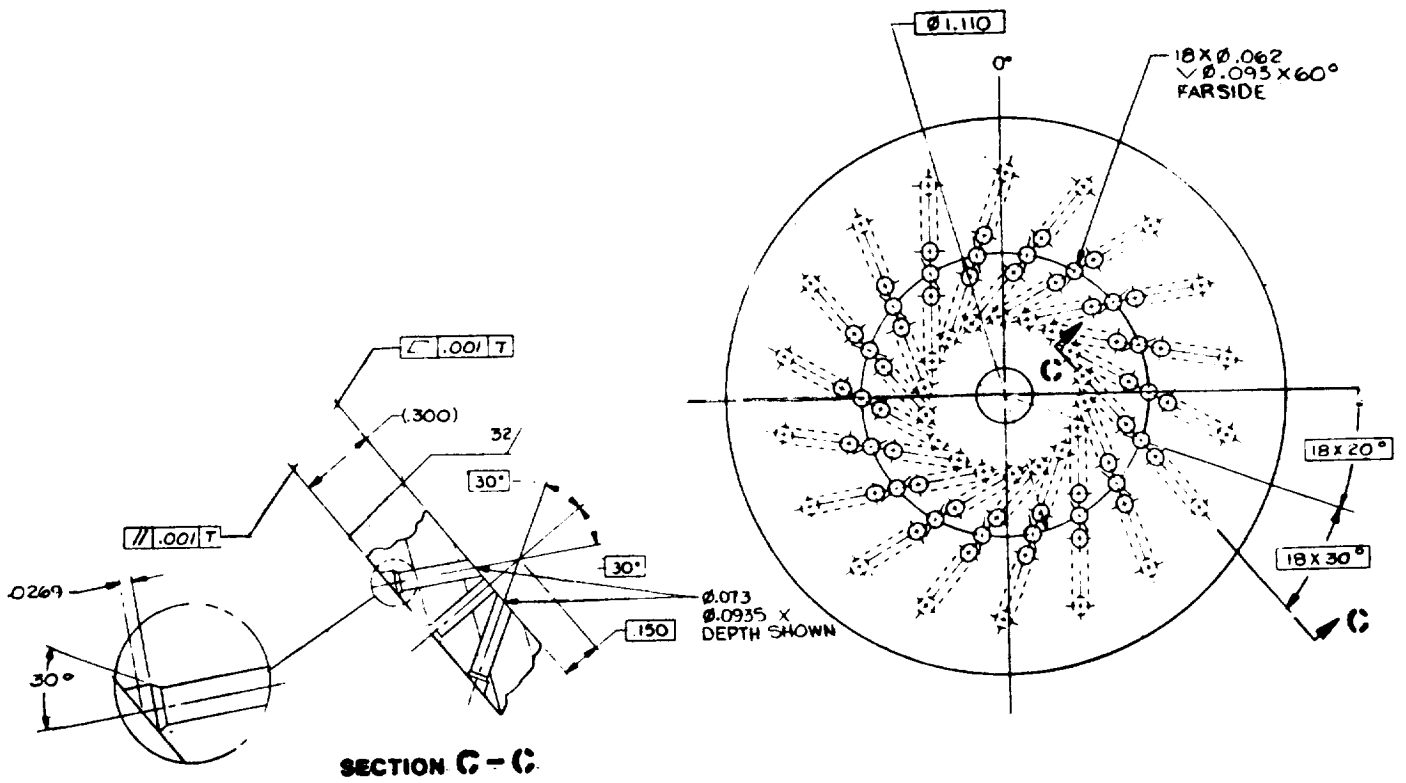


Figure 12. High Injection Density Injector

4.3, Injector Mixing Experiments (cont.)

supercritical fluid or liquid injection. The flow Reynolds number based on either the injector orifice diameter or the chamber diameter was approximately 10 to 100 times lower than that for an actual gas generator (which are approximate 10^6 to 10^7), but still was fully turbulent. The effect of Reynolds number is considered negligible on the tests conducted.

The measured mixing data (i.e. the relative concentration distributions) indicate large regions of unmixed fuel and oxidizer. The observed mixing is less than that required to suppress soot particle formation. The conclusion drawn from the test data is that finite rate mixing effects on soot particle inception exist with conventional gas generator design.

4.3.1 Test Apparatus

The test apparatus is shown in Figure 13 and a schematic diagram is shown in Figure 14. The high injection density injector S/N 1202756 was mounted vertically on a test stand with the propellant simulants supplied from high pressure supply tanks. The flowrates were set using calibrated sonic orifices. The green light output (514 nm) from a 5 watt argon ion laser was focused into a sheet 1.5 in (3.7 cm) wide directed across the flow. A diagnostic chamber (not shown in the schematic) was mated to the injector to prevent entrainment of surrounding air. The design of the diagnostic chamber is shown in Figure 15. The 12-inch long chamber has two long axial slots on opposite sides to permit the sheet of laser light to be introduced across the flow anywhere along the length of the chamber. At 90 degrees to the sheet are 1.0-inch diameter windows located to collect the scattered laser light. The chamber contains four axial passages for heated water to maintain a constant chamber temperature (approx. 50 C) during testing to prevent condensation on the inside windows.

The laser light scattered off the Freon molecules was imaged onto a gated image intensifier with a 2:1 demagnification ratio. The image intensifier was gated on for approximately 10 microseconds using a TTL triggering circuit. The image intensifier provides a gain of approximately 1000 to the scattered light intensity. The 10 microsecond "exposure time" is sufficiently short to freeze the flow field and provide an instantaneous image of the mixing. The output of the image intensifier was imaged onto an RS-170 format video camera which was triggered to take a single frame when the intensifier was gated on. The video image was then digitized by a VS-100 frame grabber and then uploaded to an Apollo DN10000 workstation for processing and storage.

ORIGINAL PAGE
BLACK AND WHITE PHOTOGRAPH

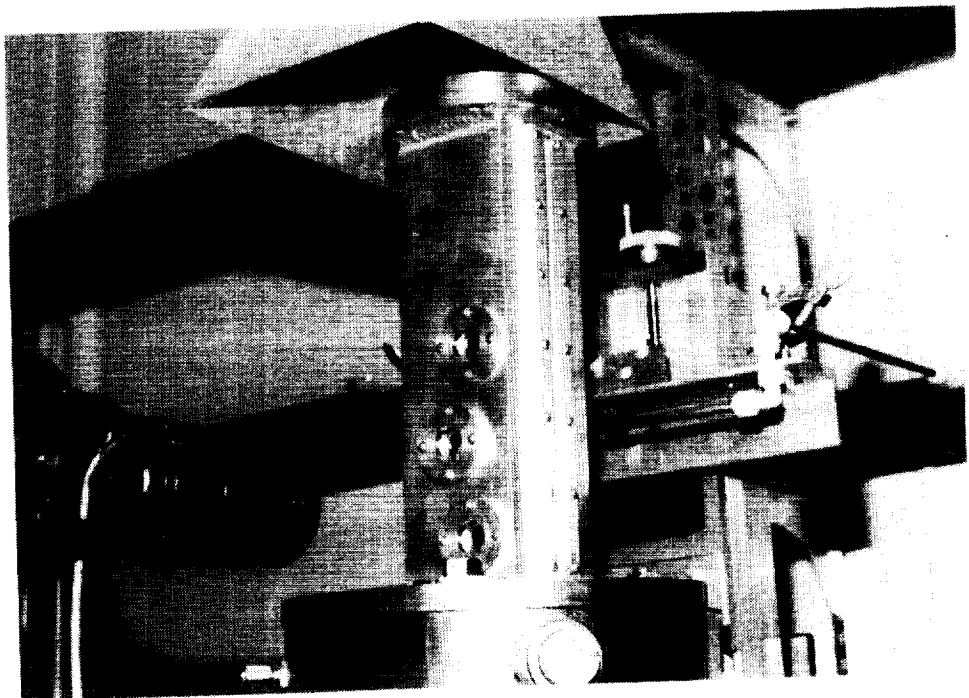
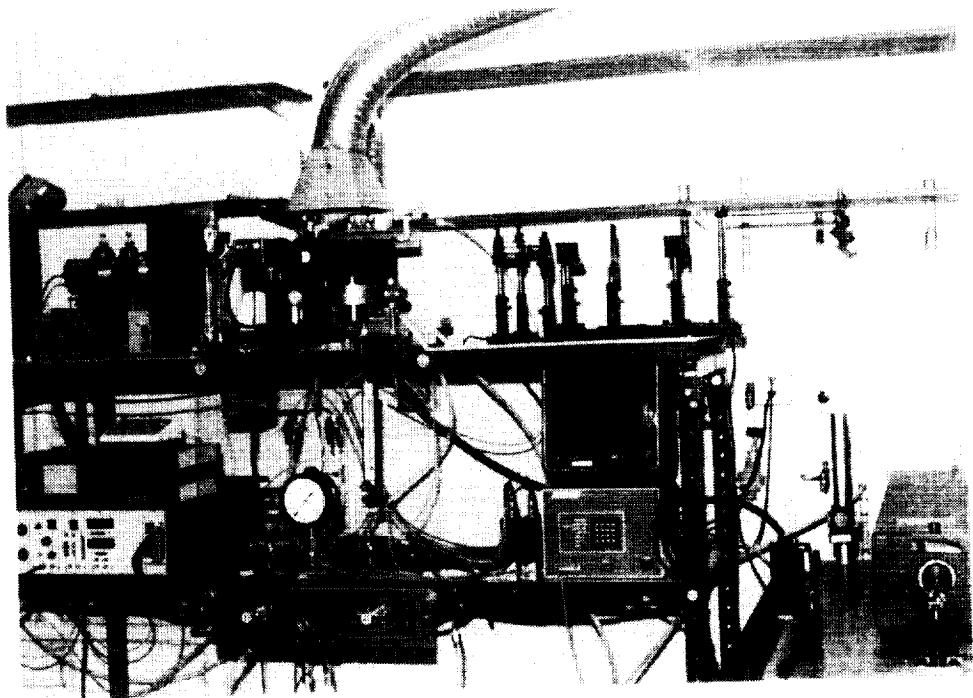


Figure 13. Test Apparatus For Injector Mixing Tests

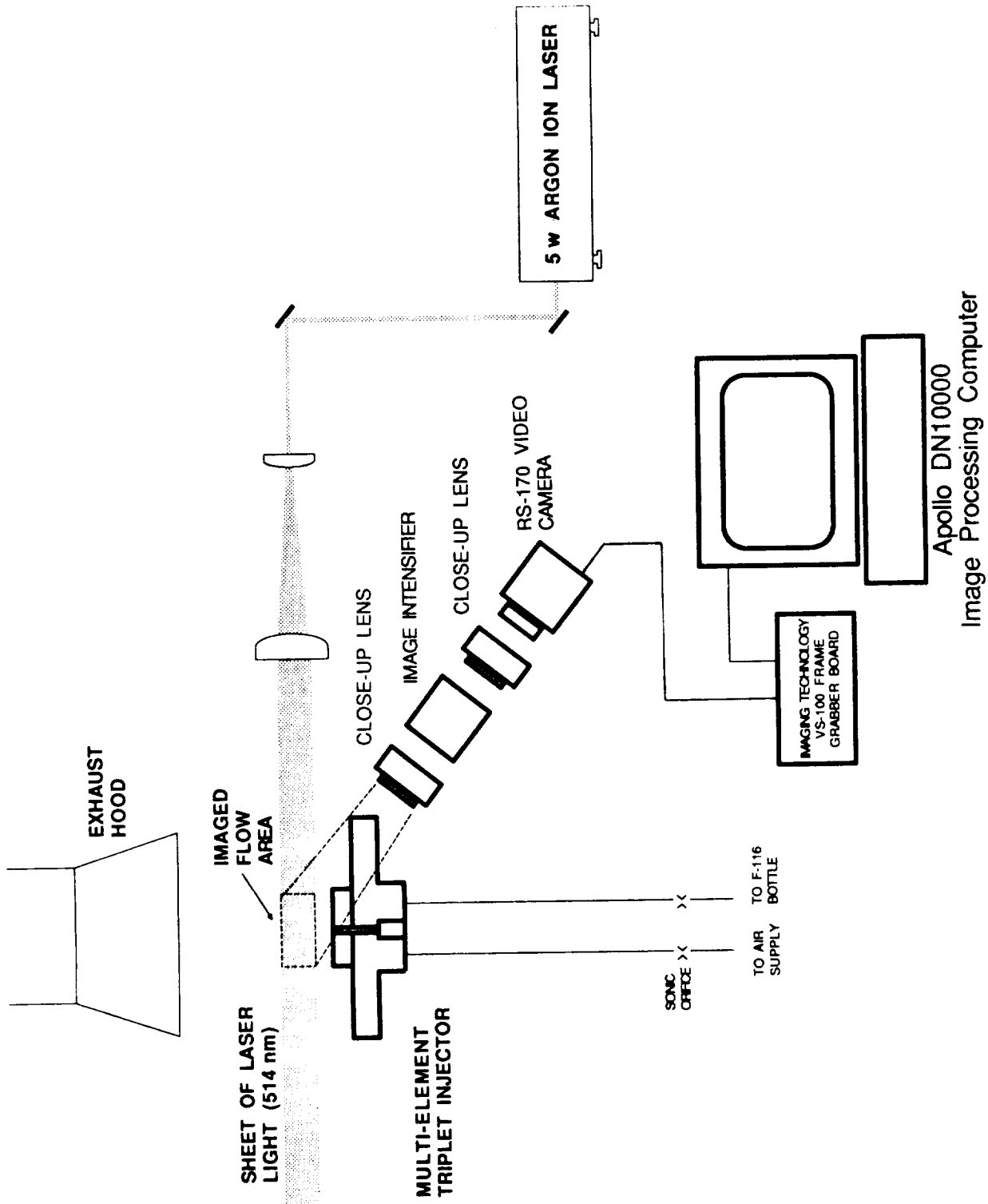
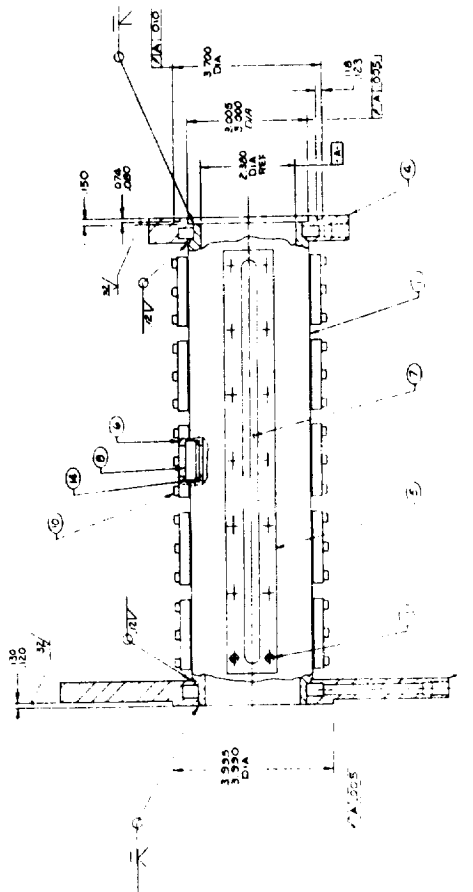


Figure 14. Experimental Apparatus For 2-D Rayleigh Scatter Imaging of Injector Mixing

- 1. INTERPRET DRAWING PER ATC 31C-4326
- 2. QUANTITY PER ATC 46231
- 3. WELDING METHOD PER MIL-STD-883C
- 4. DIMENSIONS PER METHOD A AND D PER A PER
- 5. DIMENSIONS PER METHOD B PER MIL-STD-883C
- 6. DIMENSIONS PER METHOD C PER MIL-STD-883C
- 7. MAKE PER AS478-30 NITS (20442) AND
- 8. APPLICABLE DASH NO.



INFORMATION ONLY
DO NOT FABRICATE
UNLESS APPROVED BY
APPLICABLE AUTHORITY
APPROVED BY: [Signature]

3 A125Y

NO.	DESCRIPTION	QTY	UNIT	REVISION
1	MIL STD 20 P 500 1/4 DIA			
2	WOODRUFF DRUMS			
3	PARKER SEAL OF ESJUV			
4	MIL STD 20 P 500 1/4 DIA			
5	MIL STD 20 P 500 1/4 DIA			
6	MIL STD 20 P 500 1/4 DIA			
7	MIL STD 20 P 500 1/4 DIA			
8	MIL STD 20 P 500 1/4 DIA			
9	MIL STD 20 P 500 1/4 DIA			
10	MIL STD 20 P 500 1/4 DIA			
11	MIL STD 20 P 500 1/4 DIA			
12	MIL STD 20 P 500 1/4 DIA			
13	MIL STD 20 P 500 1/4 DIA			
14	MIL STD 20 P 500 1/4 DIA			
15	MIL STD 20 P 500 1/4 DIA			
16	MIL STD 20 P 500 1/4 DIA			
17	MIL STD 20 P 500 1/4 DIA			
18	MIL STD 20 P 500 1/4 DIA			
19	MIL STD 20 P 500 1/4 DIA			
20	MIL STD 20 P 500 1/4 DIA			
21	MIL STD 20 P 500 1/4 DIA			
22	MIL STD 20 P 500 1/4 DIA			
23	MIL STD 20 P 500 1/4 DIA			
24	MIL STD 20 P 500 1/4 DIA			
25	MIL STD 20 P 500 1/4 DIA			
26	MIL STD 20 P 500 1/4 DIA			
27	MIL STD 20 P 500 1/4 DIA			
28	MIL STD 20 P 500 1/4 DIA			
29	MIL STD 20 P 500 1/4 DIA			
30	MIL STD 20 P 500 1/4 DIA			
31	MIL STD 20 P 500 1/4 DIA			
32	MIL STD 20 P 500 1/4 DIA			
33	MIL STD 20 P 500 1/4 DIA			
34	MIL STD 20 P 500 1/4 DIA			
35	MIL STD 20 P 500 1/4 DIA			
36	MIL STD 20 P 500 1/4 DIA			
37	MIL STD 20 P 500 1/4 DIA			
38	MIL STD 20 P 500 1/4 DIA			
39	MIL STD 20 P 500 1/4 DIA			
40	MIL STD 20 P 500 1/4 DIA			
41	MIL STD 20 P 500 1/4 DIA			
42	MIL STD 20 P 500 1/4 DIA			
43	MIL STD 20 P 500 1/4 DIA			
44	MIL STD 20 P 500 1/4 DIA			
45	MIL STD 20 P 500 1/4 DIA			
46	MIL STD 20 P 500 1/4 DIA			
47	MIL STD 20 P 500 1/4 DIA			
48	MIL STD 20 P 500 1/4 DIA			
49	MIL STD 20 P 500 1/4 DIA			
50	MIL STD 20 P 500 1/4 DIA			
51	MIL STD 20 P 500 1/4 DIA			
52	MIL STD 20 P 500 1/4 DIA			
53	MIL STD 20 P 500 1/4 DIA			
54	MIL STD 20 P 500 1/4 DIA			
55	MIL STD 20 P 500 1/4 DIA			
56	MIL STD 20 P 500 1/4 DIA			
57	MIL STD 20 P 500 1/4 DIA			
58	MIL STD 20 P 500 1/4 DIA			
59	MIL STD 20 P 500 1/4 DIA			
60	MIL STD 20 P 500 1/4 DIA			
61	MIL STD 20 P 500 1/4 DIA			
62	MIL STD 20 P 500 1/4 DIA			
63	MIL STD 20 P 500 1/4 DIA			
64	MIL STD 20 P 500 1/4 DIA			
65	MIL STD 20 P 500 1/4 DIA			
66	MIL STD 20 P 500 1/4 DIA			
67	MIL STD 20 P 500 1/4 DIA			
68	MIL STD 20 P 500 1/4 DIA			
69	MIL STD 20 P 500 1/4 DIA			
70	MIL STD 20 P 500 1/4 DIA			
71	MIL STD 20 P 500 1/4 DIA			
72	MIL STD 20 P 500 1/4 DIA			
73	MIL STD 20 P 500 1/4 DIA			
74	MIL STD 20 P 500 1/4 DIA			
75	MIL STD 20 P 500 1/4 DIA			
76	MIL STD 20 P 500 1/4 DIA			
77	MIL STD 20 P 500 1/4 DIA			
78	MIL STD 20 P 500 1/4 DIA			
79	MIL STD 20 P 500 1/4 DIA			
80	MIL STD 20 P 500 1/4 DIA			
81	MIL STD 20 P 500 1/4 DIA			
82	MIL STD 20 P 500 1/4 DIA			
83	MIL STD 20 P 500 1/4 DIA			
84	MIL STD 20 P 500 1/4 DIA			
85	MIL STD 20 P 500 1/4 DIA			
86	MIL STD 20 P 500 1/4 DIA			
87	MIL STD 20 P 500 1/4 DIA			
88	MIL STD 20 P 500 1/4 DIA			
89	MIL STD 20 P 500 1/4 DIA			
90	MIL STD 20 P 500 1/4 DIA			
91	MIL STD 20 P 500 1/4 DIA			
92	MIL STD 20 P 500 1/4 DIA			
93	MIL STD 20 P 500 1/4 DIA			
94	MIL STD 20 P 500 1/4 DIA			
95	MIL STD 20 P 500 1/4 DIA			
96	MIL STD 20 P 500 1/4 DIA			
97	MIL STD 20 P 500 1/4 DIA			
98	MIL STD 20 P 500 1/4 DIA			
99	MIL STD 20 P 500 1/4 DIA			
100	MIL STD 20 P 500 1/4 DIA			

Figure 15. Diagnostic Chamber Assembly (page 1 of 2)

ORIGINAL PAGE IS
OF POOR QUALITY

4.3, Injector Mixing Experiments (cont.)

4.3.2 Test Summary

A test summary of the injector mixing experiments is shown in Table II. The tests simulate mixture ratios from .25 to 0.5. The first five tests used 2-D imaging of the Rayleigh scattering from Freon 116 to obtain instantaneous maps of the species concentrations. The spatial gradients in the concentrations have been used to estimate the mixing. During the second five tests the flow was seeded with alumina particles (approximately 1 micron diameter) and laser doppler velocimetry measurements of the axial velocity and turbulence intensity at locations of high concentration gradient were made. For the LDV measurements the chamber was rotated 90 degrees and the LDV beams were introduced through the circular window and the doppler signal collected in the forward scattering angle by a photomultiplier. The LDV measurements were processed using a TSI Burst Doppler Counter and data reduction software.

Rayleigh scattering of light is a linear process where the scattered light is at the same frequency as the incident light. In addition, the intensity of the scattered light is linearly proportional to the concentration of the scattering molecules in the probe volume (or sheet.) Freon 116 and air were chosen as the simulants because the Rayleigh scattering from the Freon is approximately 10 times that for air. The relative concentrations of the fuel simulant were obtained using the procedure described below.

Calibration of Video System

The variations in pixel sensitivity of the camera and the optical efficiency of the lens/intensifier system were calibrated using an image taken with stagnant air. Because the concentration is uniform, variations in pixel sensitivity, optics losses, and power variations in the laser sheet can be detected on the image. These variations were found to be no greater than 25%. The test images acquired were corrected for this variation by normalizing the data, by dividing the digitized intensity reading by the value of the calibration image.

Determination of Mixture Fraction

In order to compare the results of the cold flow mixing with previous work on soot particle suppression, the relative concentration of the fuel simulant must be expressed in terms of a mixture fraction, ξ . As defined in eq. 42 below, the mixture fraction varies between 1 (pure fuel) to 0 (pure oxidizer).

Table II. Injector Mixing Test Results

Test No.	Laser Power (w)	Laser Sheet Width (mm)	Mass Flow Fuel (lbm/s)	Mass Flow Ox (lbm/s)	Re(d) Fuel	Re(d) Ox	ρ Fuel	ρ Ox	Re(D)	Al ₂ O ₃ Seeding	Scalar Dissipation Rate (sec ⁻¹)	Turbulence Intensity (%)
1	5	40	0.035	0.011	13240	13315	0.160	0.257	25287	No	0.09	-----
2	5	40	0.042	0.011	15888	13315	0.192	0.257	29135	No	0.14	-----
3	5	40	0.031	0.019	11727	22999	0.142	0.444	27486	No	0.14	-----
4	5	40	0.042	0.019	15888	22999	0.192	0.444	33533	No	0.15	-----
5	5	40	0.051	0.025	19292	30262	0.233	0.585	41778	No	0.14	-----
6	5	-----	0.035	0.011	13240	13315	0.160	0.257	25287	Yes	-----	35
7	5	-----	0.042	0.011	15888	13315	0.192	0.257	29135	Yes	-----	46
8	5	-----	0.031	0.019	11727	22999	0.142	0.444	27486	Yes	-----	56
9	5	-----	0.042	0.019	15888	22999	0.192	0.444	33533	Yes	-----	61
10	5	-----	0.051	0.025	19292	30262	0.233	0.585	41778	Yes	-----	63

4.3, Injector Mixing Experiments (cont.)

$$\xi = Z_{fi}/Z_f \quad (42)$$

Z_f = overall mass fraction of fuel

$$= ((1/MR + 1)MR)^{-1}$$

Z_{fi} = local mass fraction of fuel

= % of Full Scale light detected

False color images of the relative fuel concentration at MR=0.3 and MR=0.5 are shown in Figure 16. The impinging jets of fuel can be seen on each side of the injector. The mixing shown is in the axial direction, perpendicular to the injector face. The effect of the injectors swirl design can be seen in the upper instantaneous image by the appearance of larger fuel jets on the left side of the the images where the fuel is being sprayed into the laser sheet. On the right side of the image the fuel jets appear smaller, even though they are the same size as those on the left side, because the fuel is being sprayed away from the laser sheet. A large recirculation zone in the center of the injector is readily apparent. The size of this zone may be exaggerated due to the absence of an igniter flow. In general, significant mixing does not appear to occur until at least 20 injection orifice diameters (approximately 1.5 in) downstream of the injector face.

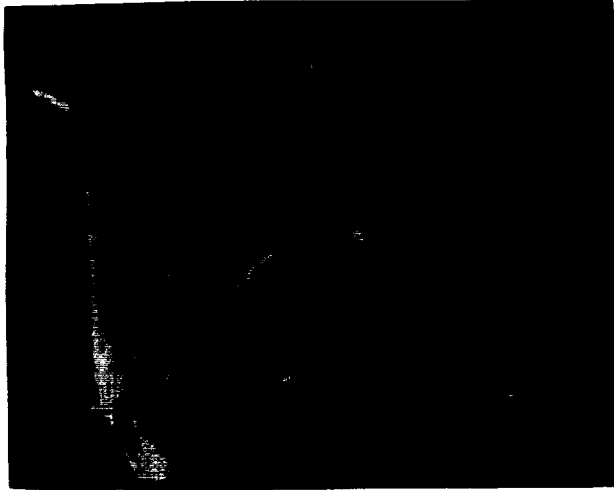
Determination of Mixing Rate

The relevant turbulent mixing parameter for soot formation is the mean scalar dissipation rate (the scalar is the mixture fraction ξ) defined in eq. 43,

$$\bar{\chi} = 2D(\nabla\xi)^2 \quad (43)$$

where D is the binary diffusion coefficient for air and Freon 116. The scalar dissipation rate is a measure of the concentration gradient between the fuel and the oxidizer. A high value of the rate implies rapid mixing. The dissipation rate varies throughout the flow field. To characterize the entire flow properly by a single average value, a volume weighted average value must be used. Such an average can be obtained by analyzing several transverse and axial images through the flow. A complete survey of the flow such as this was beyond the scope of this investigation.

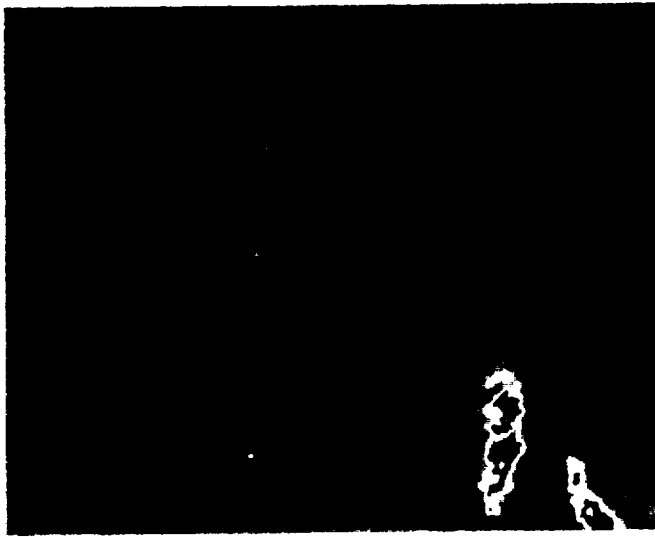
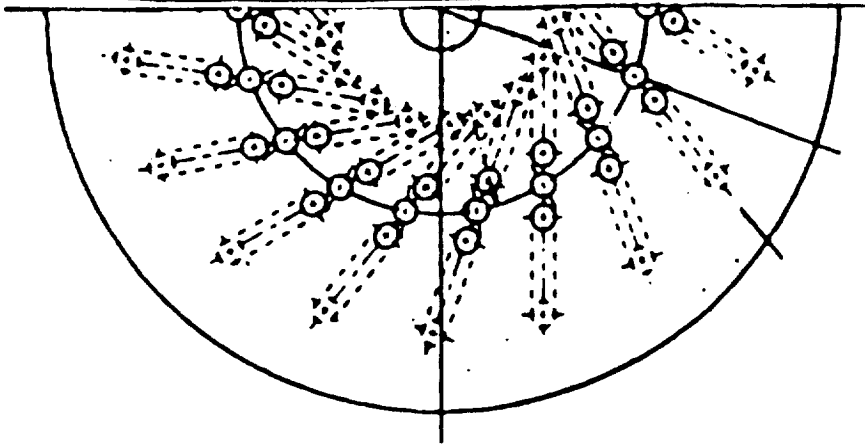
An estimate of the average dissipation rate in the primary mixing zone, approximately 5 orifice diameters from the injector has been made. The calculated scalar dissipation rate at this location is reported in Table II. While no data are available for the



Instantaneous Image

MR=0.3

(Colors Not Proportional
To Concentration)



Time Averaged Image

MR=0.5

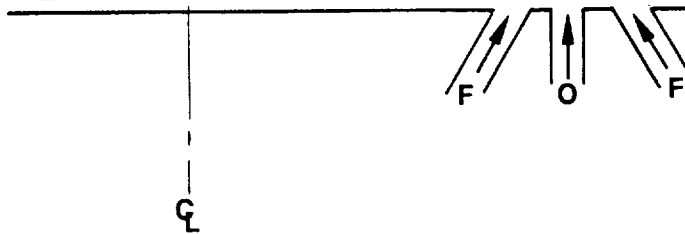


Figure 16. 2-D Images of Injector Mixing at MR=0.3 and MR=0.5

4.3, Injector Mixing Experiments (cont.)

dissipation rate which causes suppression of soot particles from oxygen/RP-1, Kennedy [24] has measured a value of 0.85 sec^{-1} for air/propane. The values measured during the cold flow testing are approximately 15 to 20% of this value. In addition, LDV measurements of the axial velocity were made at the same location as the calculated scalar dissipation rates and they indicate high turbulence intensities based on the axial velocity component. The average turbulence intensity, which ranged from 35 to 63 % (based on 1200 measurements) are reported in Table II. Typically, high turbulence levels correlate with increased mixing. Further investigation of injector designs to generate even higher turbulence levels and greater mixing is indicated by the results of these tests. Injector designs which substantially promote mixing and short combustion lengths such as a HIPERTHIN or swirl vortex designs should provide conditions for less soot formation.

4.4 MODEL VALIDATION PROGRAM

A model validation program has been defined (1) to provide data to validate the current Low Mixture Ratio Combustion and Carbon Deposition Model, (2) to use the model to design an advanced LO_2 /hydrocarbon gas generator, and (3) to use the test data to further the development of a CFD based soot formation and deposition model. The time phasing and synergism between specific tasks is shown in Figure 17. The empirical variables required to complete and validate the current model are shown in Figure 18. The primary data required are (1) axial profiles of the soot concentration (i.e. soot volume fraction), (2) soot particle number densities under well-defined mixing conditions and (3) soot deposition and soot layer adhesion strength measurements. The recommended test program consists of three tiers of testing starting with bench scale testing, then high pressure single element testing, and then subscale (1/2 to 1/10 scale) hot fire testing.

4.4.1 Validation Program Tasks

Controlled Low Mixture Ratio Combustion Tests

Currently, little fundamental combustion data exists for very fuel rich oxygen/RP-1 and oxygen/propane flames. In particular, the effects of fuel composition (purity and additives), fuel pyrolysis reaction paths, soot surface growth rates, and soot deposit characteristic are unknown. The initial task of the validation program should be a series of controlled low MR combustion experiments to address these issues. The objective of these tests is to obtain sufficient data with RP-1 and propane at low mixture ratio conditions so the basic hypotheses and theories of

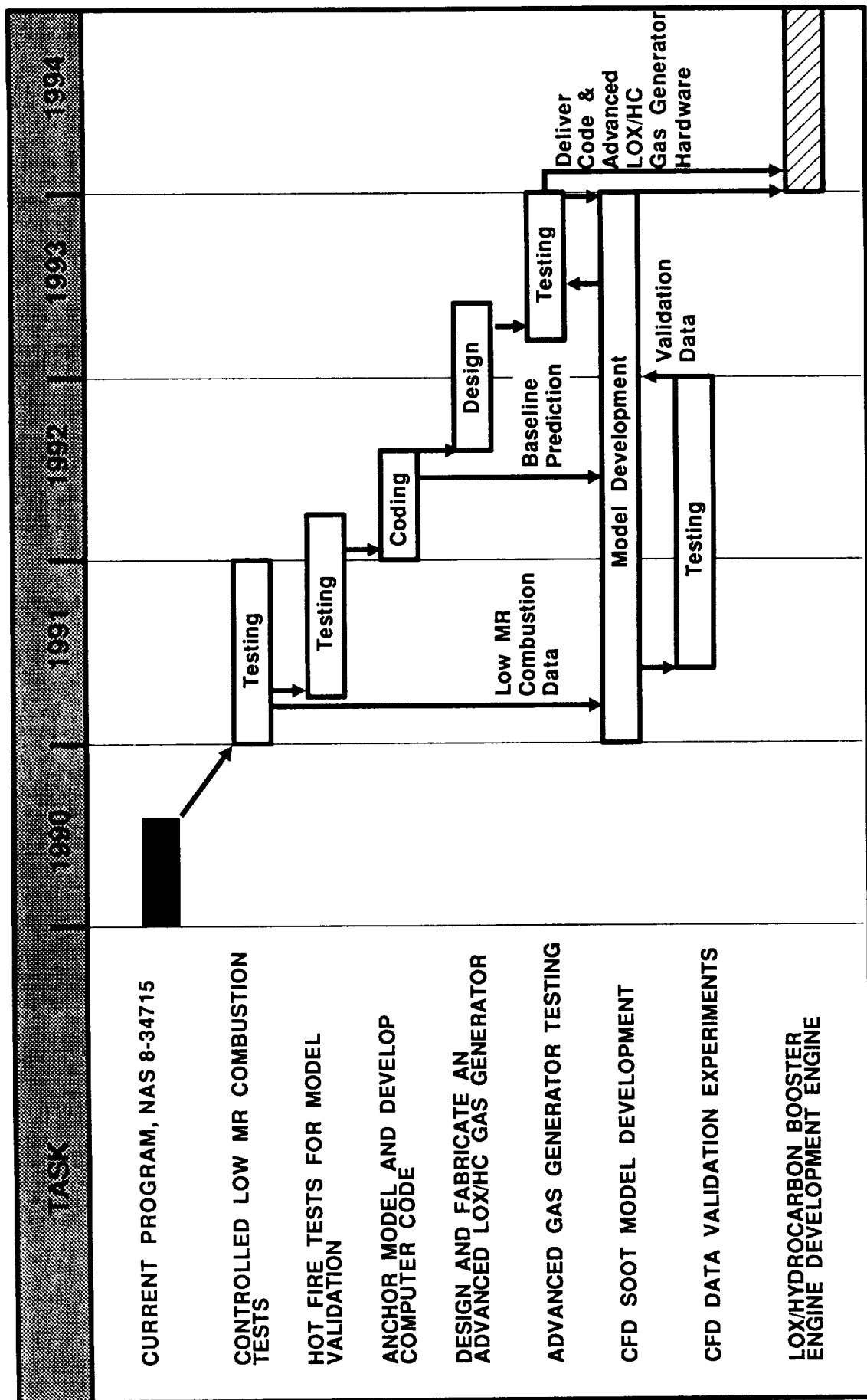


Figure 17. Model Validation Program

SOOT VOLUME FRACTION:
$$\phi_s(t) = \left[(V_s N_s)^{1/3} + \frac{C}{\beta N_s^{2/3}} \{ (N_s \beta t + 1)^{2/3} - 1 \} \right]^3$$

SOOT SURFACE GROWTH RATE REACTION:
$$C = d \left(\frac{c}{o} \right)^n \exp \left\{ \frac{E_a}{R} \left(\frac{1}{T_m} - \frac{1}{T_c} \right) \right\}$$

SOOT NUMBER DENSITY:
$$N_o = \epsilon_m(x) \cdot \frac{x}{v} \cdot K_1 \cdot \exp \left(-c_1 \frac{x}{L} \right)$$

NET SOOT DEPOSITION:
$$j_{sm}^* = (1-R) \phi_s \rho_s v St_{sm} \left(\frac{-B}{1-\epsilon} \right)^{-D}$$

SOOT REMOVAL FRACTION:
$$R = P(\tau \geq F_{sd}) = \frac{1}{\sqrt{2\pi}} \int_{\ln(x^* - \eta)/\sigma}^{\infty} \exp\left(-\frac{k^2}{2}\right) dk$$

EMPIRICAL QUANTITY	MODEL VARIABLE	REQUIRED DATA	PROPOSED TESTS	REQUIRED DIAGNOSTICS
Soot Surface Growth Rate	C	Soot Volume Fraction and Particle size as a function of MR, pressure for each fuel of interest in a flame with a known flow field.	Laminar premixed and counter flow diffusion flame measurements at 1, 10, and 100 atm pressure with each fuel for 0.25 < MR < 1.5	Laser Extinction - Soot Volume Fraction Rayleigh Scattering- Particle Size Thermocouple Rate
Soot Particle Number Density	N _o	Soot Volume Fraction and Soot Particle size as a function of relative velocity between fuel jet and an oxidizer jet. Also relation of local distribution to 1-D average.	Single element injector tests at elevated pressure a multielement tests at low and then high pressure. The flow fields mapped using cold flow imaging and LDV.	LDV - Velocity Rayleigh Scattering - Mixing Rayleigh Scattering- Particle Size Laser Extinction- Soot Volume Fraction
Constants For Mixing	K ₁ , c ₁ , K ₂	Soot Volume Fraction and Soot Particle size as a function of time, pressure, and M.R.	Axial measurements of soot volume fraction and particle size down length of subscale gas generator	Laser Extinction - Soot Volume Fraction Rayleigh Scattering- Particle Size
Thermophoretic Deposition Force,	D	Measurement of deposition and Soot Volume Fraction in a well defined turbulent flow field with controlled wall temperatures	Hot Fire Subscale GG tests using single cooled cylinder in cross flow. Map upstream flow with LDV. Measure deposition and soot volume fraction.	LDV - velocity field Extinction - Soot Volume Fraction Deposition Measurement Thermocouple Rate
Soot Deposit Strength	K _{50%}	Measurement of predicted vs actual deposition to determine over a wide range of fluid shear stress values	Bench top experiments using a laminar stagnation point flow to determine fluid shear stress at which soot reentrainment occurs. Later results can be correlated subscale deposition measurements.	Extinction - Soot Volume Fraction Deposition Measurement

Figure 18. Data Requirements for Model Validation

4.4, Model Validation Program (cont.)

soot formation and deposition used to develop the model can be verified. The fundamental questions to be addressed in the tests are:

1. Is the amount of solid carbon formed by liquid fuel coking negligible compared to the soot produced by gas phase reactions?
2. Do the soot particles stop growing at a size of 200 nm, so that thermophoresis governs the deposition? Do the particles undergo additional agglomeration and form particles larger than 1 micron in diameter?
3. What is the soot surface growth rate for RP-1 and are values which have been measured for air/propane at equivalence ratios from $\Phi=1$ to 2, valid for oxygen/propane at $\Phi=9$ to 12?
4. What is the effect of fuel purity on the soot surface growth rate?
5. What are the major intermediate species and final combustion products resulting from low MR RP-1 and propane combustion?
6. What is the soot layer adhesion strength for RP-1 and propane?

Insight into these fundamental questions can be achieved through three types of controlled bench scale tests. It is recommended that the tests be conducted with RP-1, propellant grade propane, research grade dodecane, and high purity grade propane. The latter two fuels should be included in the testing to assess fuel blend effects.

The model uncertainties regarding coking, particle size, and combustion species can be reduced by making measurements in the first type of test setup illustrated in Figure 19, an under ventilated diffusion flame. The required test apparatus consists of an enclosed vessel with optical access such as the diagnostic chamber used in the cold flow experiments. A simple spray atomizer or coax injection port is used to form a turbulent diffusion flame within the vessel at the desired mixture ratio. Because the flame is fuel rich, the flame height is relatively short compared to a normal diffusion flame and the flame will spread out to the side walls of the chamber as illustrated in Figure 19. Optical measurements of soot particle size and gas sampling measurements can be made throughout the flow. The particle size measurements (Rayleigh and Mie scattering) indicate whether the solid carbon is due to soot formation or liquid fuel coking.

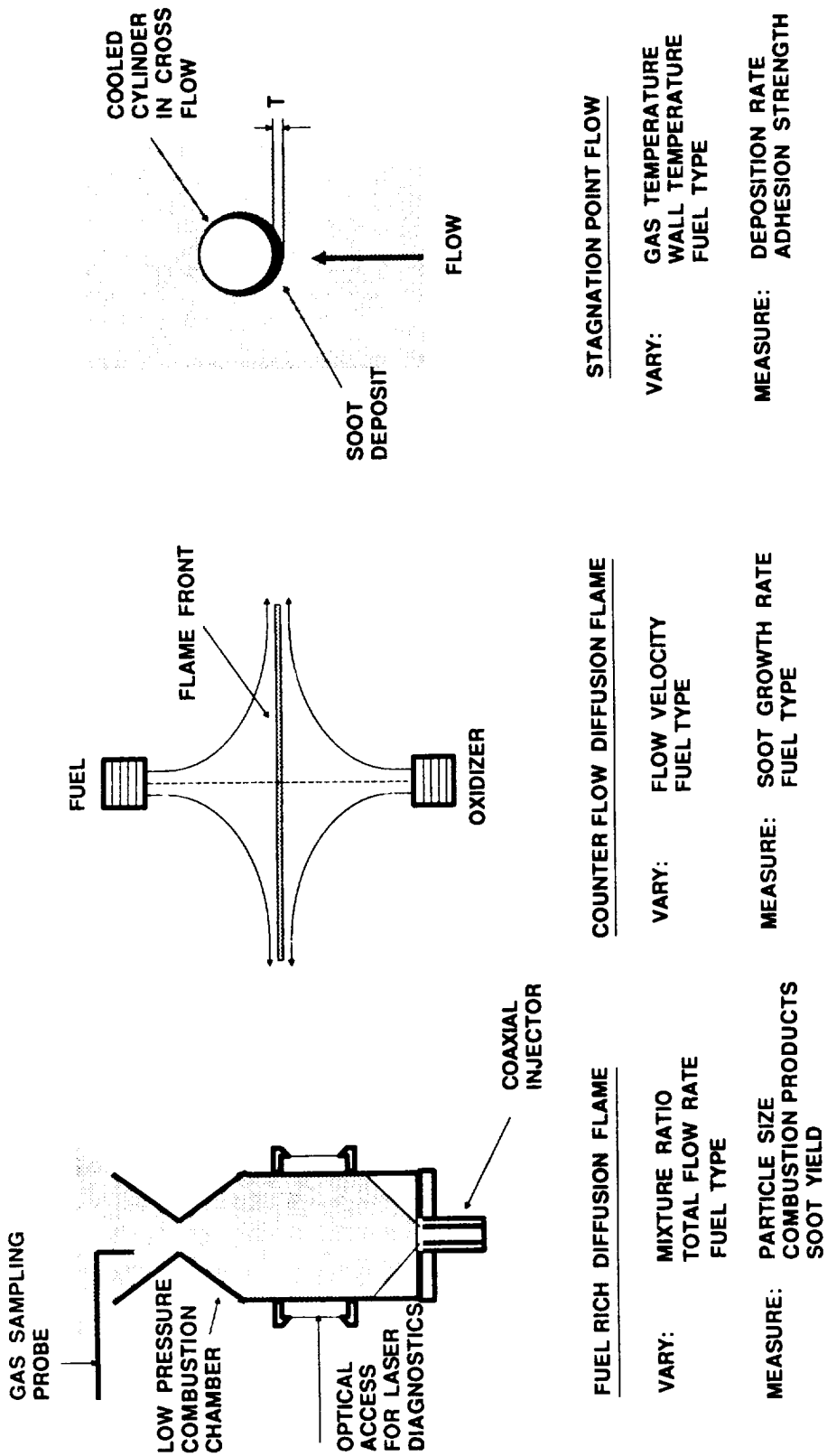


Figure 19. Controlled Low Mixture Combustion Tests

4.4, Model Validation Program (cont.)

The gas sampling measurements using a gas chromatography analysis can identify the species to be included in the combustion kinetics model.

The soot surface growth rate, soot particle inception rate, and fuel composition effects can be determined using a counter flow diffusion flame [24,27] as shown in Figure 19. In this configuration, fuel and oxidizer flows are directed at each other forming a stationary flame front at the stagnation point. The rate of mixing and soot particle residence time can be controlled by adjusting the propellant flow rates. The soot surface growth rate can be found by measuring the soot volume fraction, particle residence time, and flame temperature.

The soot deposit adhesion strength can be determined by measuring the soot deposition from a hot sooty flow across a cooled cylinder, as shown in Figure 19. The wall shear stress can be controlled by adjustment of the flow rate of the hot gas. The cylinder wall temperature can be varied by adjusting the cooling on the inside of the cylinder. Measurement of the airborne soot volume fraction and the deposition rate can be made using the two color laser measurement techniques described in section 4.4.2. From this type of test, both the thermophoretic correlation for soot deposition and the soot deposition adhesion strength model can be validated.

The results from the controlled low mixture ratio combustion tests should provide sufficient data to insure that all important processes have been included in the model. In addition, some empirical parameters in the model can be quantified. The results should provide sufficient insight into the remaining uncertainties in the model, such that an efficient hot fire test program can be designed to "fill in" the voids and validate the model. In addition, the data obtained should be very helpful in developing a CFD base soot formation and deposition model as described below.

Hot Fire Tests For Model Validation

While the controlled low MR tests described above are adequate to verify the physics of the model and quantify some variables, validation requires direct comparison of the model prediction to subscale test data. Two types of tests are recommended for model verification. The first type of tests are single element injector tests to screen candidate injector designs and to determine the correlation between the mixing, soot number density, and local temperature variations. These tests would use a small high pressure single element injector and chamber designed to

4.4, Model Validation Program (cont.)

accommodate optical access such as that used on the Photographic Combustion Characterization of LOX/Hydrocarbon Type Propellants, NAS9-15724 [22] and shown in Figure 20. Single element injector testing at realistic injection densities and pressures (1000 to 2000 psia) offers a good compromise between realistic combustion conditions, diagnostic accessibility, and cost. The primary objective of these tests should be to develop a database on injector design effects.

The second type of testing is subscale (1/10 to 1/2 scale) gas generator testing such as that which was conducted during Task V of the program. The modular hardware designs developed on this program are ideal for the subscale testing. Additional components for making the required diagnostic measurement could be incorporated in the test setup. A test matrix would be run where the mixture ratio, pressure, and total flow rate would be varied for at least two injector designs selected from the single element injector testing. Measurements of the soot volume fraction, soot particle size, gas temperature, and deposition at different axial locations would be made. The data would provide the basis for anchoring the model.

Anchor Model and Develop Computer Code

The results of tests described above would be used to produce a final anchored version of the model. The equations for the soot formation, deposition, flow, and combustion kinetics would be programmed into a FORTRAN computer code and a detailed user's manual would be prepared. Parametric analyses using the model would be conducted to identify gas generator designs offering the potential to minimize carbon deposition.

Design, Fabricate and Test an Advanced LO₂/Hydrocarbon Gas Generator

Based on the results of the parametric analysis, the detailed design of an advance gas generator should be initiated. The objective of this effort would be to demonstrate the use of the model for developing new gas generator designs. Currently, the design of a new gas generator is a significant risk because of the uncertainty in extrapolating from the limited number of existing designs. To overcome carbon deposition effects, the design of an advanced gas generator may be a significant departure from current designs. Testing of the prototype advanced gas generator would be conducted and the results compared to the predictions of the model. At the conclusion of this effort the anchored code and prototype hardware would be delivered to NASA for use as the baseline design in a future LO₂/hydrocarbon engine development program.

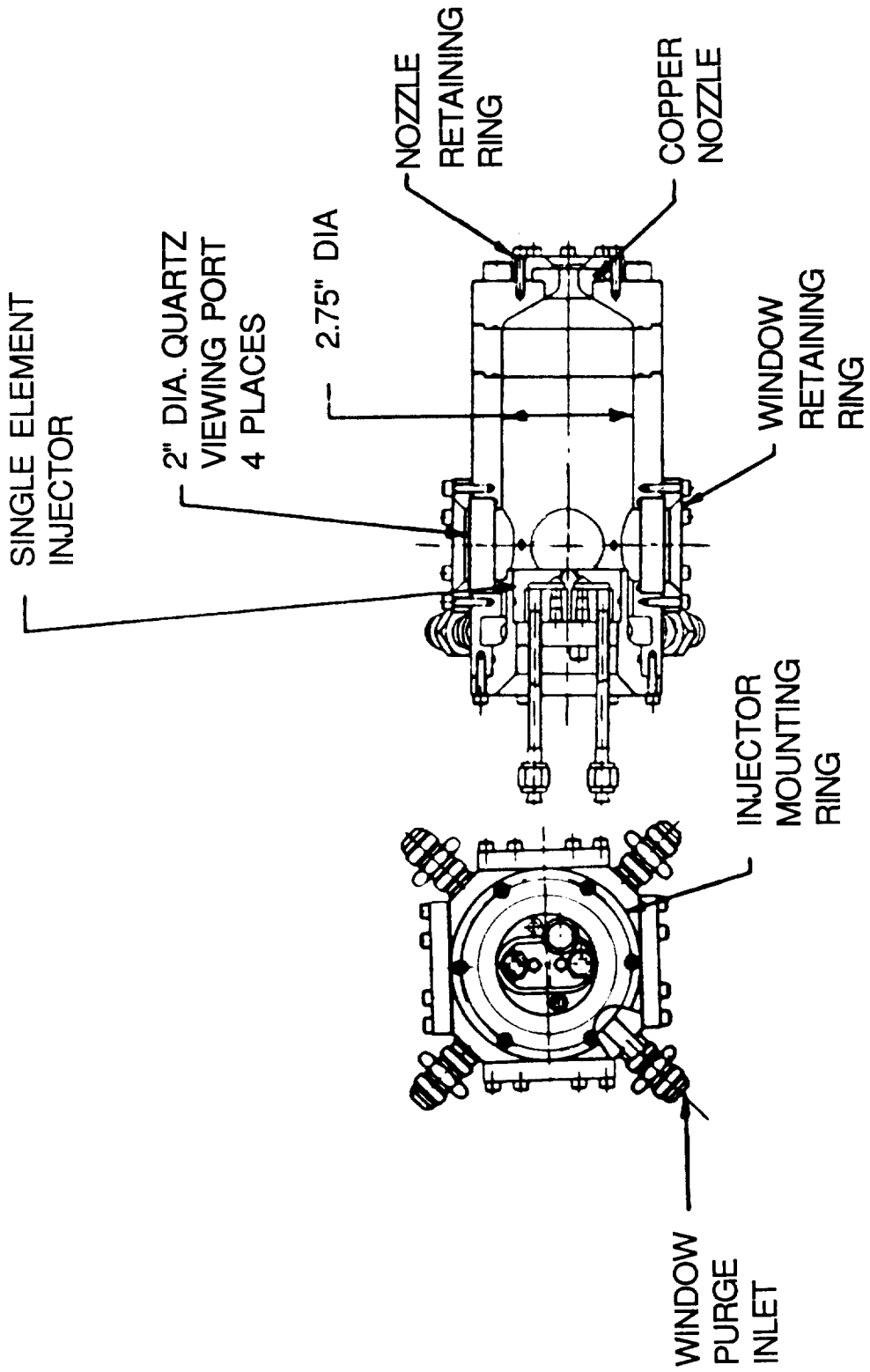


Figure 20. Single Element Injector Testing

4.4, Model Validation Program (cont.)

CFD Soot Model Development and Supporting Experiments

Development of a second generation soot formation and deposition model using CFD techniques should be initiated. CFD is emerging as a powerful tool for analysis of turbulent reacting flows in complex geometries. The extension of Level III type models, reviewed in Section 4.1.2, from "classical" flame configurations to rocket engine combustion CFD codes appears feasible. The objective of this task would be to modify an existing rocket engine CFD code (e.g. Aerojet's BICOMB, FLUENT, etc.) with a submodel to account for soot formation, transport, and deposition. The principle task will be to develop a workable turbulent closure scheme for the soot formation source terms in the soot particle conservation equation (eq. 1). Existing turbulence modeling schemes such as k- ϵ and algebraic stress models are suitable for modeling the remaining terms in the equation. A robust CFD based model would reduce the major uncertainties introduced by the empirical correlations used in the 1-D model.

Data to validate the CFD based model can be obtained from the controlled low mixture ratio combustion tests and additional support experiments specifically designed support the CFD model. The additional support experiments would consist primarily of mapping the combustion flow to obtain both time averaged and instantaneous measurements of the velocity, temperature, and the injector spray. Such detailed measurements are not required to validate the 1-D empirical model, but are needed to validate the flow field predictions produced by a CFD based model. The CFD model offers greater potential applicability and accuracy than the empirical 1-D model. The disadvantage of the CFD approach is that it may not yield a reliable gas generator design tool in the near future. Alternatively, the empirical 1-D model developed in this study should be readily achieved through the test program described above.

4.4.2 Diagnostics and Hardware Requirements

Validation of model will require measurement of the soot parameters, discussed in Section 4.3.2, in the controlled low MR combustion tests and the hot fire validation tests. In order to measure the parameters indicated in Figure 18, nonintrusive diagnostics will be required. A summary of potential diagnostics is given in Table III and described in detail below. The diagnostics have been evaluated based on capability, complexity, and use in a hot fire test program. In addition to the nonintrusive diagnostics listed, secondary measurements of pressure, temperature, and species concentrations using conventional instrumentation and gas sampling are assumed to be available during testing and are not discussed in detail.

Table III. Review of Diagnostics For Model Validation Testing

DIAGNOSTIC TECHNIQUE	TYPE	PARAMETER MEASURED	MODEL VARIABLES	SPATIAL RESOLUTION	HARDWARE ACCESS	MATURITY	COST
Extinction	NONINTRUSIVE	Soot Volume Fraction	C, ϕ, N_o	LINE-OF-SIGHT	LOW	HIGH	LOW
Scattering	NONINTRUSIVE	Soot Particle Size	K_1, c, C	POINT	MODERATE	HIGH	LOW
Two-Color Deposition	NONINTRUSIVE	Soot Volume Fraction & Deposit Thickness	$D, K_{50\%}$	POINT	LOW	HIGH	LOW
LDV	NONINTRUSIVE	Flow Velocity	K_1, c, N_o	POINT	MODERATE	HIGH	MODERATE
LIF	NONINTRUSIVE	OH and CH Concentration	C, N_o	Pt, 1-D, 2-D	MODERATE	MODERATE	HIGH
CARS	NONINTRUSIVE	Major Species & Temperature	K_2	POINT	MODERATE	MODERATE	VERY HIGH
Gas Sampling	DISTRUBS FLOW	Stable Species	Kinetics Model	POINT	HIGH	HIGH	MODERATE
Temperature Rakes	DISTRUBS FLOW	Bulk Temperature	N_o, K_2	MULTIPLE POINTS	HIGH	HIGH	LOW

4.4, Model Validation Program (cont.)

Laser Extinction

The average soot volume fraction along a line-of-sight can be measured from the attenuation of laser power of a beam which passes through a sooty gas flow. The extinction (attenuation) of the laser beam power is primarily due to the absorption of light by soot particles. Rayleigh scattering of laser light from soot particles typically accounts for less than 1 percent of the total power loss and its contribution is neglected in determining the soot volume fraction [37]. In the dense spray region near the face of the injector, attenuation of laser light due to scattering and absorption by unburned fuel droplets can occur. The effect of droplets along the beam path length can be accounted for by measuring the extinction at two separate frequencies. The ratio of the attenuated laser beam power, I , to the incident power, I_0 , is given by eq. 44.

$$I/I_0 = \exp(-k_{\text{ext}}L) \quad (44)$$

where: k_{ext} = Extinction Coefficient

L = Path Length

The procedures for determining the average soot volume fraction along the line-of-sight of the beam is to first determine the extinction coefficient, k_{ext} . The incident laser power, I_0 , and the path length, L , are assumed known as indicated on Figure 21a. The attenuated power, I , is measured with a photodiode and the extinction coefficient is calculated directly from eq. 44. The soot volume fraction is related to the extinction coefficient by eq. 45.

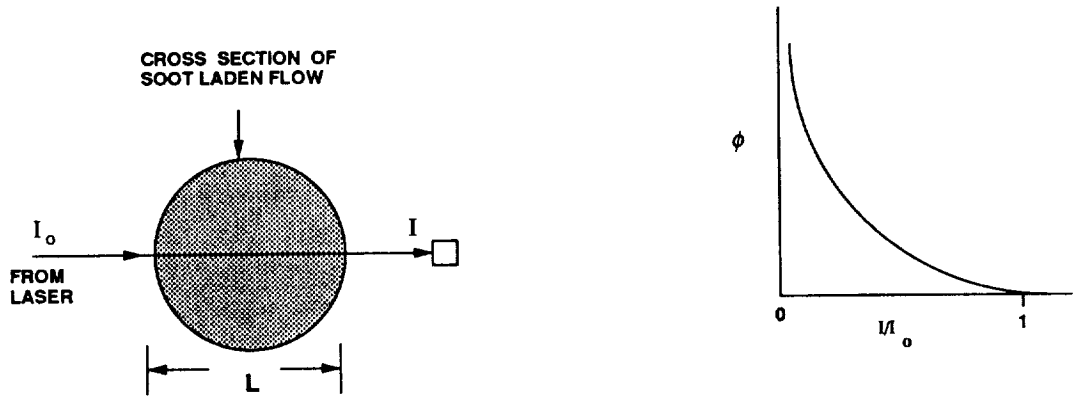
$$\phi = \frac{\lambda_o}{6\pi \text{Im} \left[\frac{(n^2 - 1)}{(n^2 + 2)} \right] k_{\text{ext}}} \quad (45)$$

where: λ_o = wavelength of laser

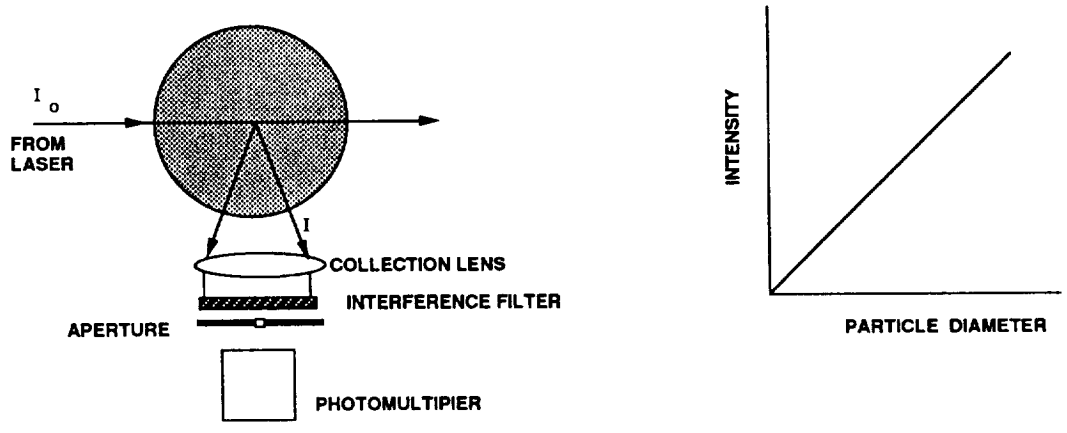
n = refractive index of soot

$$= 1.54 - 0.57i$$

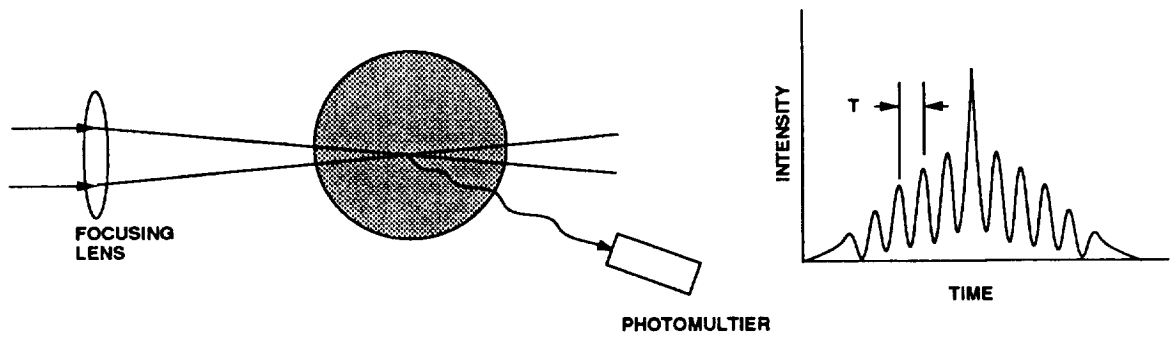
A large attenuation corresponds to a large extinction coefficient and a large soot volume fraction as illustrated in Figure 21a.



(a) Laser Extinction

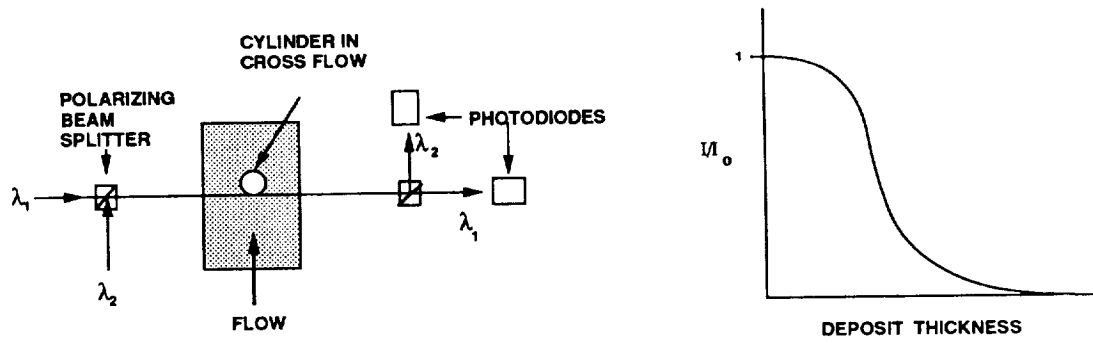


(b) Rayleigh Scattering

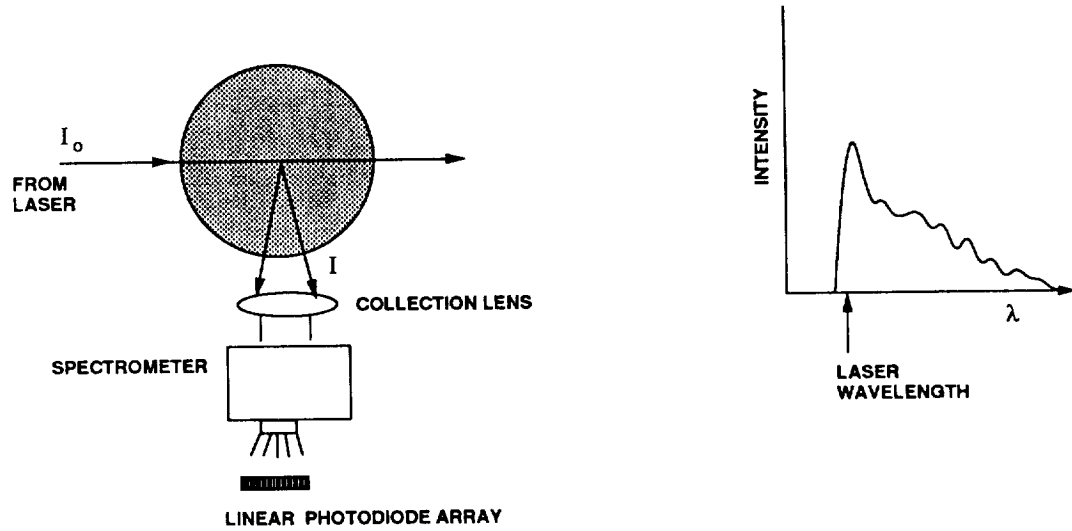


(c) Laser Doppler Velocimetry

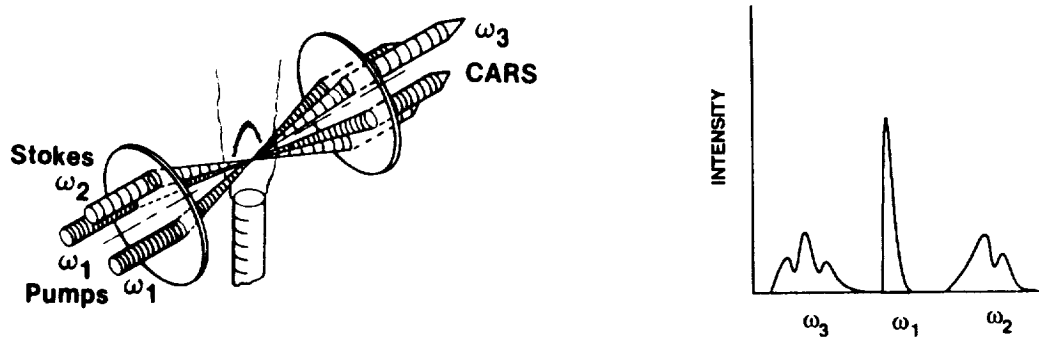
Figure 21. Fundamentals of Laser Diagnostics for Model Validation



(d) Two Color Deposition Measurement



(e) Laser Induced Fluorescence



(f) Coherent Anti-Stokes Raman Spectroscopy

Figure 21. Con't

4.4, Model Validation Program (cont.)

Laser extinction has been used extensively for the past 15 years to study soot formation. The technique has also been used on large scale combustion devices such as diesel engines [38] and gas turbine engines [26]. The technique requires only limited optical access (5 to 10 mm diameter windows). The laser source for the technique is a relatively inexpensive, continuous-wave (cw) argon ion laser with from 3 to 5 watts of power.

Rayleigh Scattering

Rayleigh scattering of laser light is an elastic scattering process, the scattered light is at the same frequency as the incident light. Rayleigh scattering occurs from both molecules and small particles where the wavelength of light, λ , and the particle diameter, d_p , are $\pi d_p / \lambda < 1$. For particles where $50 > \pi d_p / \lambda > 1$, the elastic scattering is governed by Lorentz-Mie theory. For soot particles the elastic scattering is typically assumed to be Rayleigh scattering [33, 39]. Measurement of the Rayleigh scattered light in combination with a laser extinction measurement can be used to determine the soot particle number density and the average soot particle size.

A typical setup for a Rayleigh scattering measurement is shown in Figure 21b. Scattered light from a small segment of length, l , of the laser beam is collected by a lens and focused into a photomultiplier detector. Light scattered off unburned fuel and oxidizer droplets (typically larger than 10 microns) can be distinguished by monitoring the scattered light at a second angle (e.g. 45 degrees). Since Rayleigh scattered light (vertically polarized) scatters equally in all directions and Mie scattered light (from large particles) does not scatter uniformly, the Rayleigh signal can be extracted by monitoring both detectors and rejecting data when the signal differ. The intensity of the Rayleigh scattered light, I , is proportional to the number density of soot particles in the probed volume (typically 1 mm^3) as given by eq. 46.

$$I = C I_0 N \Omega l (ds/d\Omega) \quad (46)$$

where:

C= Collection Efficiency

I_0 =Incident Laser Intensity

N= Soot Number Density

Ω =Solid Collection Angle

4.4, Model Validation Program (cont.)

l = length of probe volume

$(ds/d\Omega)$ = Scattering Cross Section of Soot

The scattering cross section for soot can be derived as eq.47 [37].

$$(ds / d\Omega) = \frac{8\pi}{3} \left(\frac{2\pi\lambda}{n} \right)^4 |\gamma|^2 \quad (47)$$

where:

λ = laser wavelength

n = refractive index for soot

$$\gamma = \frac{d_p}{8} \left(\frac{n^2 - 1}{n^2 + 2} \right)$$

The soot extinction coefficient, k_{ext} , determined from a simultaneous laser extinction measurement, is related to the average particle diameter through the extinction efficiency, Q_{ext} , as given in eq. 48.

$$Q_{ext} = \frac{k_{ext}}{N} \left(\frac{4}{\pi d_p^2} \right) \quad (48)$$

The extinction efficiency is the ratio of the extinction cross section to the geometric cross sectional area of the soot particle. The extinction efficiency is equal to the sum of the absorption efficiency and the scattering efficiency as given in eq. 49.

$$Q_{ext} = Q_{abs} + Q_{sca} \quad (49)$$

For Rayleigh scattering particles with a complex refractive index the absorption and scattering efficiencies can be shown as given in eqs. 50 and 51 [37].

$$Q_{abs} = \frac{8\lambda}{d_p^2} \text{Re}(i\gamma) \quad (50)$$

$$Q_{sca} = 4(ds / d\Omega) / (\pi d_p^2) \quad (51)$$

4.4, Model Validation Program (cont.)

Equations 47, 48, 49, 50, and 51 can be solved to determine the average soot particle diameter, d_p , and the soot particle number density, N . A map of the soot number density through the flow can be determined by scanning the beam through the flow and adjusting the focus of the detection optics.

Rayleigh scattering has been used extensively in fundamental soot formation studies [21,26] and in combustors. This will be the primary diagnostic technique used to determine the soot particle number density at inception and to determine the soot surface growth reaction rate.

Laser Doppler Velocimetry (LDV)

Laser Doppler velocimetry (LDV) techniques have been developed for measuring mean and instantaneous velocity components and turbulent velocity parameters. Commercially available "turn-key" systems are available and have been applied to a wide range of practical combustion devices [36]. A typical cross beam LDV configuration is shown in Figure 20c. For a given velocity component two polarized, cw laser beams of equal strength and frequency are focused so that they cross at a point in the flow. The intersection of the beams forms a control volume typically 1 mm^3 . Within the control volume, the beams form a fringe pattern of light and dark regions due to constructive and destructive interference of the beams. A burst Doppler signal as shown in Figure 21c is detected as a particle passes through the control volume. The peaks and valleys correspond to the particle being a light or dark region. The overall shape of the signal is due to the Gaussian profile of the laser beams. Signal processing electronics are used to eliminate measurements occurring when multiple particles are in the control volume or the seed particle size is too large or too small. The flow velocity is proportional to the period of the Doppler signal as given by eq. 52.

$$U = \lambda / (2T \sin \theta) \quad (52)$$

where: λ = laser wavelength

T = period of Doppler signal

θ = half angle of intersecting beams

LDV is a mature laser diagnostic technique. Extensive data-processing software is available enabling a very large number of measurements (on the order of 1000) to be taken rapidly (1 to 10 seconds depending on the seeding rate) at a given point in the flow. Two and

4.4, Model Validation Program (cont.)

three dimensional systems configured with fiber optic probes are available, where the signal is collected through the same optics which deliver the beams. This "back scatter" configuration is the preferred arrangement (compared to the forward scatter arrangement used in the cold flow injector mixing experiment) for the hot fire test measurements, because only one optical port is required.

Laser Induced Fluorescence (LIF)

Laser induced fluorescence spectroscopy (LIF) is a technique used to measure the concentration of important combustion radical species such as OH and CH. In addition, the relative concentration of soot particle precursors (polycyclic aromatic hydrocarbons) can be measured. LIF consists of an absorption process followed by an emission process. The laser beam frequency (typically a high power, tunable, pulsed laser) is tuned to coincide with an absorption wavelength of an electronic transition of a molecule of interest. Energy from the laser is absorbed by the molecule and an electron is promoted to an excited state. Spontaneous emission and collisions of the excited molecules with other molecules causes the transition of excited electrons to lower energy states and the emission of photons (fluorescence) at the frequency characteristic of the transition. The concentration of the particles is determined by measurement of the intensity of the fluorescence at specific wavelengths.

The typical configuration for a point LIF measurement is shown in Figure 21e. The laser is tuned to a particular wavelength, λ_0 (e.g. 306.2 nm for OH,) and is focused at a point in the flow. The fluorescence signal, following the laser pulse (typically 5 to 10 mJ and 10 to 50 nsec in duration) is collected at a 90 degree angle to the beam. The collected light is then spectrally dispersed with a grating spectrometer and focused onto a linear diode array. The output of the diode array provides an instantaneous measurement of intensity versus wavelength. The technique can be extended to planar (2-D) imaging by using cylindrical lenses to expand the beam into a sheet and replacing the spectrometer and linear diode array with an intensified video camera. The filter is chosen to isolate the fluorescence at a particular wavelength. The video image then provides a map of the spatial distribution of the concentration of the particular species being probed.

LIF has been used for mapping flame location in both sooting flows[39] and spray combustion [40]. Fuel rich regions of the flow where thermal decomposition of the fuel

4.4, Model Validation Program (cont.)

forms soot precursors can be identified by fluorescence of the CH radical which is present in these regions. Fluorescence of the OH under low mixture ratio combustion conditions indicates the location of oxidizer rich portions of the flow (i.e. oxidizer streaks). The use of LIF on the single element injector tests can provide a hot fire assessment of injector mixing efficiency. Comparison of the results for different injector configurations may lead to the design of an injector element which minimizes the soot formation rates.

Two Color Soot Deposition Measurement

Simultaneous measurement of soot volume fraction and deposition thickness is possible using a two color laser diagnostic technique [30]. The technique has been used to measure soot deposition rates from hot gas flows to cooled cylinders in crossflow. The technique uses two colinear cw laser beams of different frequency. The technique is illustrated in Figure 21d. The beams are superimposed on one another and are aligned so that they pass tangent to a surface where the deposition will be measured. As soot builds up on the surface, the beams are partially blocked. The beams are separated (either by color or polarity) after they pass through the flow and the attenuated power is measured. The soot volume fraction can be determined as is described above for laser extinction. The additional attenuation of the signal due to physical blockage of the beam, which is proportional to the deposition thickness, is determined by comparing the attenuated signal of each laser frequency. This technique provides an on-line measurement of the deposit thickness during a test.

Coherent anti-Stokes Raman Spectroscopy (CARS)

Coherent anti-Stokes Raman spectroscopy (CARS) is a very powerful laser diagnostic technique capable of measuring the major species and temperature at a point in sooty flows. CARS is based on a non-linear, light wave mixing process capable of both high spatial and temporal resolution [41]. The technique is illustrated in Figure 21f. Laser beams at frequencies ω_1 and ω_2 , called the pump and Stokes, respectively, with a frequency difference selected for a particular molecule to be measured, are "mixed" by focusing and crossing the beams in a specific manner to generate a laser-like CARS signal beam. Temperature measurements are derived from the spectral distribution of the CARS signal beam. Concentration measurements of the probed species are determined from the intensity of the CARS signal.

4.4, Model Validation Program (cont.)

CARS is not considered a feasible diagnostic for subscale testing, but could be used for probing the near injector region in the single element testing because of its ability to work in the presence of droplets. CARS is by far the most costly and complex (both in terms of implementation and data reduction) of the potential diagnostics to be used.

Hardware Requirements:

The major hardware requirement for the validation program is the modification of existing program test hardware to accommodate optical diagnostics on subscale tests. The modular design and known combustion stability characteristics of this hardware provides an ideal apparatus for the subscale experiments. A series of "diagnostic flanges" is recommended to provide the optical access required by the diagnostics described above. These flanges would be designed to be inserted between the existing hardware components. The flanges would be water cooled and would provide a nitrogen purge flow over the windows. Three to five flanges could be used during the testing to determine the soot volume fraction, soot particle size, velocity, and soot deposition at specific locations in the gas generator.

Figure 22 illustrates a test hardware configuration using the diagnostic flange approach. For the case of multiple soot volume fraction measurements shown, a single laser source would be used to create multiple beams to be passed through the flow. The attenuated beam strength would be measured with a photodiode detector. Laser beam choppers and lock-in amplifiers would be used to maximize the signal to noise ratio. The signal from the amplifiers would then be recorded by the facility data acquisition system. The recorded voltage is proportional to the attenuated laser power.

The conceptual design of a diagnostic flange for simultaneous measurement of the soot volume fraction and velocity is shown in Figure 23. The laser beam enters on the left side of the flange and is terminated on a photodiode detector. The measured laser power is used to determine the soot volume fraction. A commercially available fiber optic, back scatter LDV probe is mounted at the bottom of the flange. The fiber optic probe is used to both deliver the beams and to collect the Doppler signal. The LDV measurement will require that the propellants be seeded with alumina particles.

The conceptual design of a diagnostic flange for direct soot deposition measurements is shown in Figure 24. The beams for the two color deposition measurement technique described above can be combined into one beam (with each color light having a different polarization). The

Sketch Not To Scale

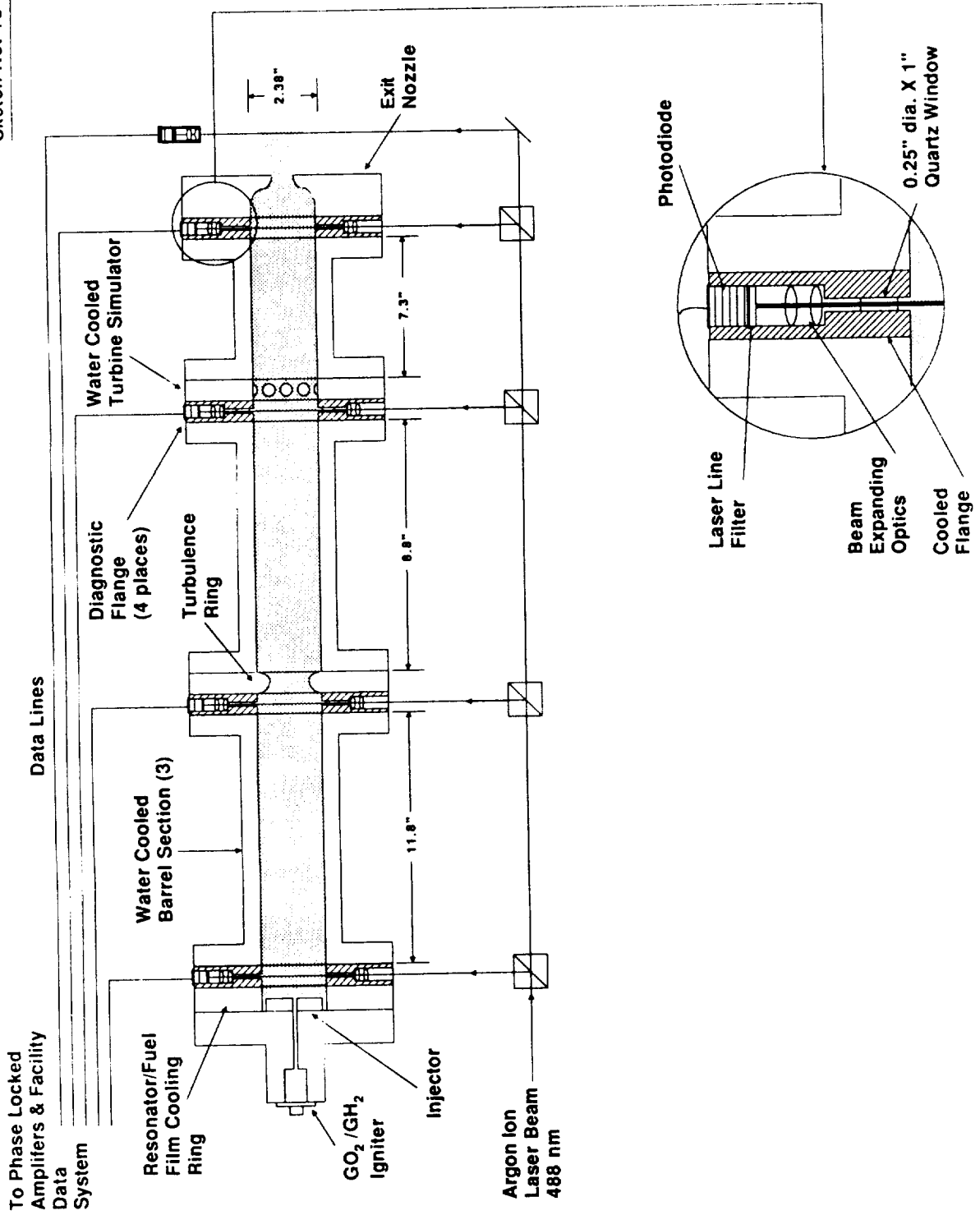


Figure 22. Subscale Hardware Configuration for Validation Testing

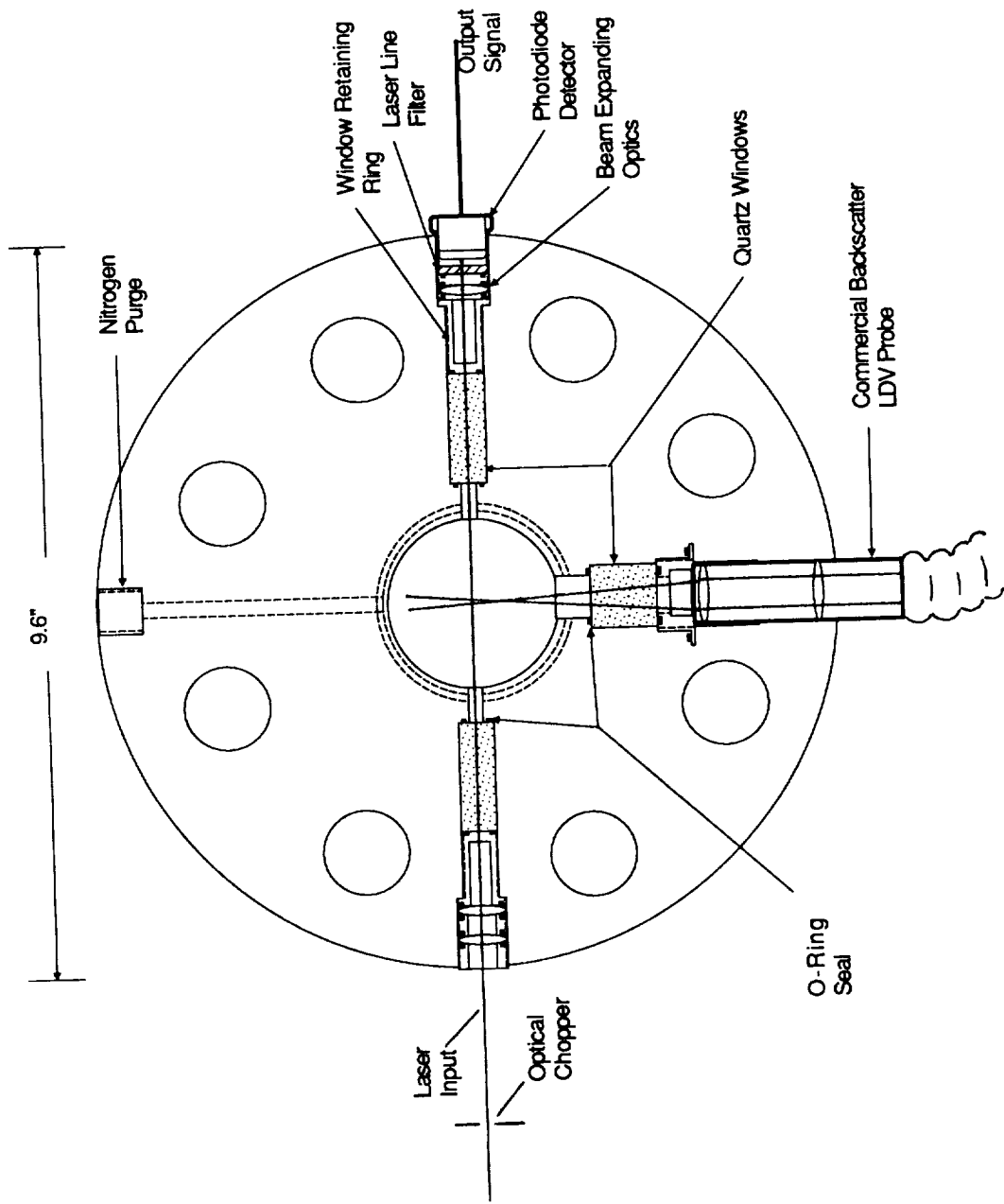


Figure 23. Conceptual Design of Diagnostic Flange for Simultaneous Extinction and LDV Measurements

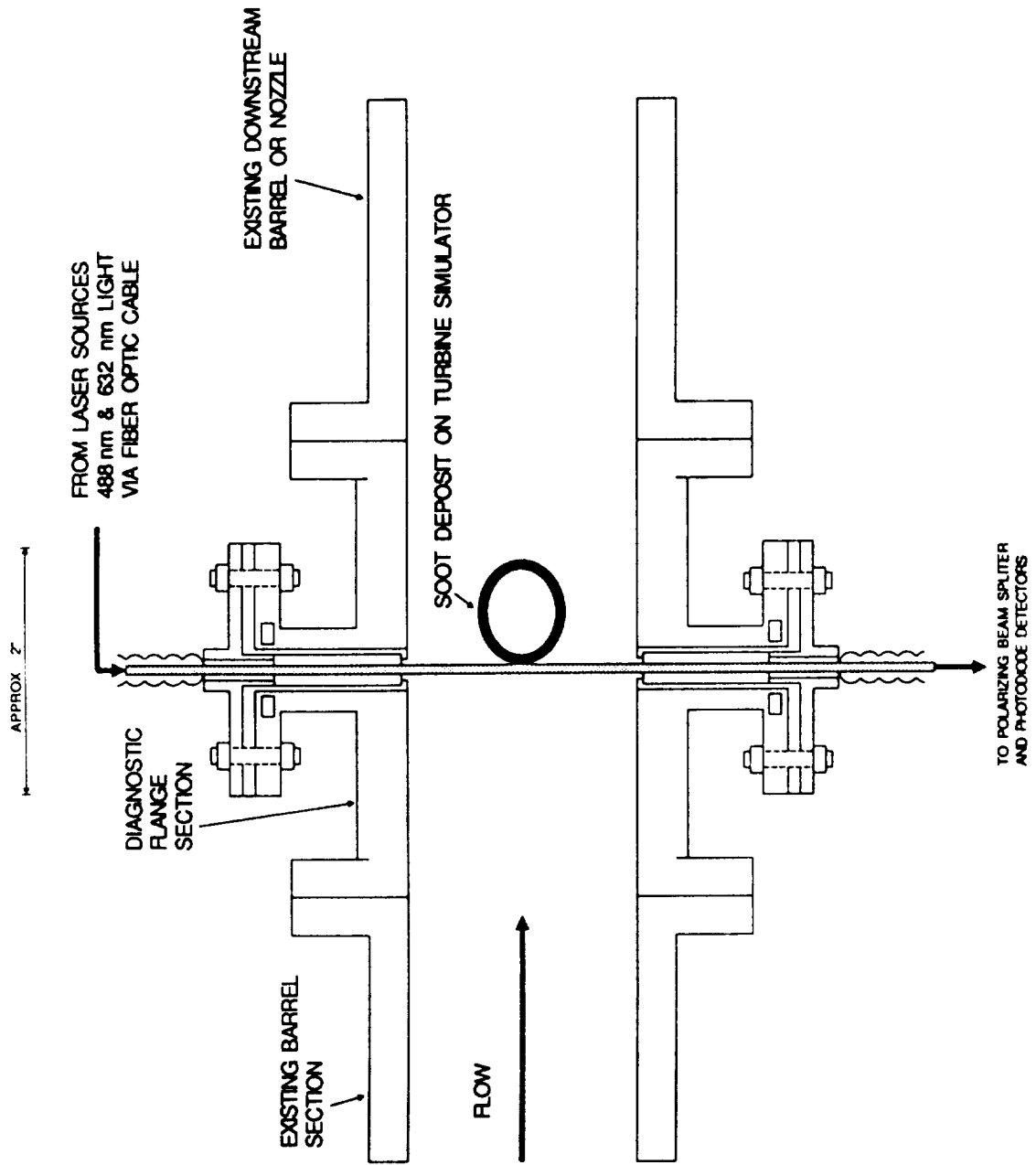


Figure 24. Diagnostic Flange for Soot Deposition Measurement

4.4, Model Validation Program (cont.)

single beam is then passed through small (0.125 inch dia.) windows, embedded in a cooled flange, on opposite sides of the gas generator. For deposition tests, the beam would pass tangent to the leading edge of a cooled surface such as the turbine simulator used in the Task V testing or a cooled cylinder in crossflow. The beams would be separated after leaving the gas generator and the attenuation for each color beam would be measured. The ratio of the attenuated signals is proportional to the soot deposit thickness. The maximum thickness which can be measured can be set by using cylindrical lenses to expand the beams into sheets from 5 to 15 mm thick or larger. The upper limit on the thickness is limited only by the size of the window access.

REFERENCES

1. Hernandez, R., Ito, J. I., and K. Y. Niiya, Carbon Deposition Model for Oxygen-Hydrocarbon Combustion, Con. NAS 8-34715, Interim Final Report 2427-IR, Sept. 1987.
2. Burkhardt, W., Niiya, K. Y., and J. A. Bossard, Carbon Deposition Model for Oxygen-Hydrocarbon Combustion, Con. NAS 8-34715, 2nd Interim Final Report 2427-IFR-2, April 1990.
3. Haynes, B. S. and H. Gg. Wagner, "Soot Formation," Prog. Energy and Comb. Sci., Vol. 7, No. 4, pp 229-273, 1981.
4. Rosner, D. E., and J. Fernandez de la Mora, "Small Particle Transport Across Turbulent Nonisothermal Boundary Layers," J. Engr. Power, Vol. 104, p. 885-894.
5. Talbot, L., Cheng, R. K., Schefer, R. W., and D. R. Willis, "Thermophoresis of Particles in a Heated Boundary Layer," J. Fluid Mech., Vol. 101, part 4, pp. 737-758, 1980.
6. Farmer, R., Edelman, R., and E. Wong, "Modeling Soot Emissions in Combustion Systems," in Particulate Carbon, Plenum Press, New York, 1981.
7. Jensen, D. E., "Prediction of Soot Formation Rates: A New Approach," Proc. R. Soc. Lond. A., Vol. 338, p.375-396., 1974.
8. Ewen, R. L., Combustion Effects on Film Cooling, Final Report, Contract NAS 3-17813, July 1975.
9. Gokoglu, S. A., and D. E. Rosner, "Prediction and Rational Correlation of Thermophoretically Reduced Particle Mass Transfer to Hot Surfaces Across Laminar or Turbulent Forced Convection Gas Boundary Layers," Chem. Eng. Commun., Vol. 44, p. 107-119, 1986.
10. Rosner, D. E., and K. Seshadri, "Experimental and Theoretical Studies of the Laws Governing Condensate Deposition From Condensing Gases," 18th. Symp. (Int.) on Combustion, The Combustion Inst., p. 1385, 1980.
11. Zimon, A. D., Adhesion of Dust and Powder, 2nd ed., translated by R. K. Johnston, Plenum Press, New York, 1982.
12. Barengoltz, J. B., "Particle Adhesion to Surfaces Under Vacuum," *J. Spacecraft*, Vol. 26, No. 2., 1989.
13. Schoenman, L., Fuel/Oxidizer-Rich, High Pressure Preburners, Final Report, NASA CR-16544, Contract NAS 3-21753, October 1981.
14. Frendklach, M., Clary, D. W., Gardiner, W. C., and Stephan Stein, "Detailed Kinetic Modeling of Soot Formation in Shock-Tube Pyrolysis of Acetylene," 20th. Symp. (Int.) on Combustion, p.887-901., The Combustion Inst., 1984.
15. Gore, J. P. and G. M. Faeth, 21st. Symp. (Int.) on Combustion, p.1521, The Combustion Inst., 1986.

REFERENCES (cont.)

16. Magnussen, B. F., and B. H. Hjertager, 16th. Symp. (Int.) on Combustion, p.719, The Combustion Inst., 1976.
17. Magnussen, B. F., and B. H. Hjertager, J. G. Olsen, and D. Bhaduri, 17th. Symp. (Int.) on Combustion, p.1383, The Combustion Inst., 1978.
18. Tesner, P. A., Snegiriova, T. D., and V. G. Knorre, *Combust. Flame*, Vol. 17, p 253, 1971.
19. Moss, J. B., Stewart, C. D., and K. J. Syed, "Flowfield Modeling of Soot Formation at Elevated Pressures," 22nd. Symp. (Int.) on Combust.,p 413, The Combustion Inst., 1988.
20. Kennedy, I. M., Kollmann, W., and J.-Y. Chen, "A Model for Soot Formation in a Laminar Diffusion Flame," to be published in *Combust. and Flame*, 1989.
21. Flower, W. L., "The Effect of Elevated Pressure on the Rate of Soot Production in Laminar Diffusion Flames," *Combust. Sci. Tech.*, Vol 48, No. 31, 1986.
22. Judd, C., Photographic Combustion Characterization of LOX/Hydrocarbon Type Propellants, Final Report, Contract NAS 9-15724, 1979.
23. Prado, G., Particulate Carbon, Plenum Press, New York, 1981.
24. Kennedy, I. M., "The Suppression of Soot Particle Formation in Laminar and Turbulent Diffusion Flames," *Combust. Sci. Tech.*, Vol. 59, pp 107-121, 1988.
25. Niel, T., and I. M. Kennedy, "Soot Formation in Ducted Turbulent Diffusion Flame," AIAA 90-0459, 26th Aerospace Sciences Meeting, Reno, NV, 1990.
26. Eckerle, W. A., and T. L. Rosfjord, "Soot Loading in a Generic Gas Turbine Combustor," *J. Prop.*, Vol. 4, No. 1, pp 89-96.
27. Axelbaum, R. L., Law, C. K., and W. L. Flower, "Preferential Diffusion and Concentration Modification in Sooting Counterflow Diffusion Flames," 22nd. Symp. (Int.) on Combust.,p 379, The Combustion Inst., 1988.
28. Hinds, W. C., Aerosol Technology: Properties, Behavior, and Measurement of Airborne Particles, Wiley-Interscience, New York, 1982.
29. JANNAF Rocket Engine Performance Methodology, CPIA Pub. 246, Johns Hopkins University, 1975.
30. Makel, D.B., and I. M. Kennedy, "Numerical and Experimental Investigation of Soot Deposition from Laminar Stagnation Point Boundary Layers," 23nd. Symp. (Int.) on Combust., The Combustion Inst., 1990.
31. Visser, J, "Adhesion and Removal of Particles II," in Fouling Science and Technology, L. F. Melo Ed., NATO ASI Series, Vol. 145, pp 105-125, 1988.

REFERENCES (cont.)

32. Nickerson, G. R., Dang., L. D., and D. E. Coats, Two-Dimensional Kinetic Reference Computer Program, Final Report, Contract No. NAS8-35931, April 1985.
33. Kays, W. M. and M. E. Crawford, Convective Heat and Mass Transfer, McGraw-Hill, New York, 1987.
34. Evans, R. M., Boundary Layer Integral Matrix Procedure, Aerotherm Division, Acurex Corp., Report Nol Aerotherm UM-75-64, Contract No. NAS8-30930, July 1975.
35. Westbrook, C. K., and F. L. Dryer, "Chemical Kinetic Modeling of Hydrocarbon Combustion," Prog. Energy Combust. Sci., Vol. 10., pp 1-57, 1984.
36. Cameron, C. D., Brouner, J., and G. S. Samuelsen, "A Model Gas Turbine Combustor with Wall Jets and Optical Access for Turbulent Mixing, Fuel Effects, and Spray Studies," 22nd Symp. (Int.), The Combustion Inst., p.965, 1988.
37. Jones, A.R., "Scattering of Electromagnetic Radiation in Particulate Laden Fluids," Prog. Energy Combust. Sci., Vol.5, pp 73-96, 1979.
38. Eckbreth, A. C., "Laser Diagnostics for Combustion Temperature and Species," Abacus Press, Cambridge, Mass., 1987.
39. Luch, R. P., Sweeney, D. W., and N. M. Laurendeau, "Laser-Saturated Fluorescence Measurements of OH Concentration in Sooty Flames," Comb. Flame, Vol. 50, pp. 189-205, 1983.
40. Allen, M.G. and R. K. Hanson, "Planar Laser-Induced Fluorescence Monitoring of OH in a Spray Flame," Opt. Eng., Vol. 25, p 1309, 1986.
41. Eckbreth, A. C., "CARS Thermometry in Practical Combustors," Comb. and Flame, Vol. 39. pp. 133-147, 1980.